

Submitted to the Astrophysical Journal

# Searching for Planets During Predicted Mesolensing Events: I. Theory, and the Case of VB 10

Rosanne Di Stefano<sup>1</sup>, James Matthews<sup>1,2</sup>, and Sébastien Lépine<sup>3,4</sup>

## ABSTRACT

The first predicted mesolensing event is likely to occur during the winter or spring of 2011/2012. The lens is the nearby, low-mass high-proper-motion star VB 10, and the source a distant field star much bluer than VB 10 and 1.5 magnitudes dimmer in B band. If VB 10 has planets, they could produce lensing signatures that enhance the detectability of the stellar-lens event and/or produce distinct planet-lens signatures. Here, we study the lensing signatures associated with planets orbiting nearby high-proper-motion stars to provide a guide for observers for this event and future predicted ones. We illustrate our case by considering hypothetical planets orbiting VB 10 with separations ranging from  $2 R_{\odot}$  to tens of AU. We find the following. (1) Wide-orbit planets can be detected for all distances of closest approach between the foreground and background stars, potentially producing independent events long before and/or after the closest approach. (2) Close-orbit planets can be detected for intermediate distances of closest approach ( $\lesssim 50$  mas for VB 10), producing quasiperiodic signatures that may occur days or weeks before and after the stellar-lens event. (3) Planets in the so-called “zone for resonant lensing” can significantly increase the magnification when the distance of closest approach is small ( $\lesssim 20$  mas for VB 10), making the stellar-lens event easier to detect while simultaneously providing evidence for planets. We show that an observing plan in which VB 10 is targeted several times per night at each of several longitudes will either detect planets, or else place weak limits on possible parameters. We expect VB 10 to be the first of a continuing line of predicted events. An observing program for this event can pave the way for future programs and discoveries. This is discussed in more detail in Paper II.

## 1. Introduction

Gravitational lensing can be used to discover planets (Mao & Paczynski 1991; Gould & Loeb 1992; Bolatto & Falco 1994; DiStefano & Scalzo 1999a,1999b; DiStefano & Night

---

<sup>1</sup>Harvard-Smithsonian Center for Astrophysics, 60 Garden Street, Cambridge, MA 02138

<sup>2</sup>School of Physics & Astronomy, University of Southampton, Southampton, SO17 1BJ, UK

<sup>3</sup>Department of Astrophysics, Division of Physical Sciences, American Museum of Natural History, Central Park West 79th Street, New York, NY 10024

<sup>4</sup>City University of New York, New York, NY

2008; DiStefano 2011). The selection effects are very different from those associated with other planet-search techniques. Lensing can therefore complement other techniques, including radial-velocity, transit, astrometric, and direct imaging studies. Furthermore, although lensing has been considered as a method that primarily discovers distant planets, we now know that it can be effective in finding planets around nearby stars as well (DiStefano 2008a, 2008b, DiStefano & Night 2008; DiStefano 2011). Nearby lenses are referred to as mesolenses. The Einstein angles and proper motions tend to be larger than typical for microlenses, producing a larger probability that a nearby system will serve as a lens, and also opening up new modes of observational study. For example, if one can extrapolate the trajectory of a nearby star, then mesolensing can be predicted in advance based on the proximity of background sources along the path. Monitoring campaigns of a type we will describe here can thus be initiated to learn more about the lens star and to explore its planetary system.

Recently, the first prediction of a mesolensing event was made (Lépine & DiStefano 2011). The event will occur when the high proper motion star VB 10 moves in front of a dim background star. In this paper we explicitly consider the full range of lensing signatures possible if VB 10 has planets. As it happens, it is likely to be challenging to observe the stellar-lens event in the VB 10 system (please see the discussion below). The complete analysis we conduct, however, determines what types of observations can help us to learn about VB 10’s planets, should they exist. More than that, we have developed a plan that can be applied to future predicted events.

VB 10 is a dwarf star, discovered by Van Biesbroeck (1944). It is particularly intriguing because its mass is estimated to be  $0.07 M_{\odot} - 0.08 M_{\odot}$ , right on the boundary separating brown dwarfs from stars. VB 10 is nearby, only 5.82 pc away, and has a proper motion of  $1.5'' \text{ yr}^{-1}$ . Because it lies in a dense region of the sky, VB 10 has a good chance of passing near a background star. For close-enough passages to a distant star, VB 10, whose Einstein ring has an angular radius of 10 milliarcseconds (mas), will serve as a gravitational lens, producing events that can be detected through an increase in light received from the background star and/or through a detectable shift in its position. One such event is likely to occur in the near future. The lensing of the background star [VB 10]-PMLS-1 (*Predicted Mesolensing Event-1*; Lépine & DiStefano 2011) by VB 10, most likely to have occurred or to occur late in 2011 or early in 2012, may turn out to be difficult to detect. The circumstances that make it challenging to detect the stellar-lens event are discussed in Lépine & DiStefano 2011. We briefly recap them below. If, however, the event can be detected and its time-scale can be measured, it will allow us to determine the gravitational mass of VB 10, providing a unique and important data point in the stellar-mass function. We do not know whether VB 10 has planets, but if it does, they may produce lensing signatures that can be more readily detected.

It is worthwhile summarizing the reasons why the VB 10 stellar-lens event is particularly challenging. Part of the reason is due to the short notice for the event. With longer notice, more high-resolution images of the area prior to the closest passage would have allowed the distance and time of closest approach to be better estimated. As it is, we have a wide window of times and distances of closest approach (Figures 1 and 2), making it difficult to plan an observing program that is well tailored to this specific event. This can be corrected for future event predictions by conducting systematic searches for possible

lens/source pairs. This will allow high-resolution images of the region to help us refine the predictions.

Part of the reason that the VB 10 event is challenging, however, is beyond human control. For example, the background star is dim (about 21 in B). Even in B, VB 10 is roughly 4 times brighter. The combination of the dimness of the background star and the brightness of the foreground star limits the ability of many observers to measure small magnifications of the background star. Furthermore, the best estimate of the time of closest approach is during the winter of 2011/2012. During this interval VB 10 is so close to the Sun that it is difficult to observe from the ground, in fact impossible to observe with some large telescopes, and is in the zone of avoidance for HST. If, however, event prediction can be accomplished on a regular basis, we should be able to identify lens/source pairs that are better suited to lensing studies. We therefore use the VB 10 event as an example to show what can be learned from monitoring the site of a predicted lensing event.

This paper is devoted to computing and illustrating the effects observers can hope to discover if VB 10 has planets. An important feature of this work is that, if the background star is monitored several times per day over the next several months, we will either find evidence of planets, or else will place weak, but quantifiable limits on the existence of planets over a wide range of orbital separations. Thus, even with the challenging circumstances described above, it is still worthwhile to monitor the region, although perhaps not as intensively as we would were the event more ideal. In fact, we will be able to derive weak limits on wide-orbit planets around VB 10, even if no discoveries are made. Of course if planets are discovered, this would be important. Whatever the results for VB 10, monitoring this system is an important step in preparing for future predictions of events that are more ideal.

The structure of this paper is structured as follows. In §2 we provide the necessary background. The lensing signatures are most directly tied to the projected distance between VB 10 and any planets it may harbor, and to the distance of closest approach. For any distance of closest approach, there is a chance that wide-orbit planets can be detected. Some detections may occur weeks or months before or after the stellar-lens event. We consider the detection of wide-orbit planets in §3.

For approaches of intermediate distance, within about 5 Einstein angles (50 mas for VB 10), close-orbit planets can be detected through small but quasiperiodic signatures that may occur days before and after the stellar-lens event, and also near the time of closest passage. We discuss the regime of close-orbit planets in §4. For approaches within about 2 Einstein angles (20 mas for VB 10), planets in the so-called “zone for resonant lensing” can significantly increase the magnification, making the stellar-lens event easier to detect while simultaneously providing evidence for planets. We devote §5 to studying the signatures expected if VB 10 has planets in the zone for resonant lensing and if the approach is close enough to allow them to be detected. The relative sizes of the regions within which lensing effects associated with each regime may be detected are shown in Figure 1, which also shows a set of possible paths of VB 10.

We conclude in §6 with an overview of how observations before, during, and after a close approach can reveal the properties of a planetary system associated with the lens star. The next step is to design observing programs that take advantage of this theoretical

work. This is the task of the companion paper (DiStefano et al. 2012, hereafter referred to as Paper II). In Paper II we give an overview of the observational approach we can use to study VB 10 during the weeks and months around the time of its close approach to the background star [VB 10]-PMLS-1. We expect VB 10 to be the first of a continuing line of predicted events. We therefore discuss the philosophy and methods of event prediction and the implications for the discovery and study of planetary systems.

## 2. Background: The Stellar-Lens Event and Possible Planetary Events

### 2.1. Sketch of Lensing Background

In this subsection we briefly sketch how the lens mass can be measured and binary and planet models can be tested. Key concepts are the Einstein angle  $\theta_E$  and the Einstein-diameter crossing time,  $\tau_E$ . The Einstein angle is defined to be the angular radius of the ring that would form the image of the source, were the source, lens, and observer to be perfectly aligned. In the absence of perfect alignment, a point lens produces two images. If  $M_*$  is the mass of the lens,  $D_L$  is the distance to the lens, and  $D_S$  is the distance to the lensed source, then

$$\theta_E = 10 \text{ mas} \left[ \left( \frac{M_*}{0.075 M_\odot} \right) \left( \frac{6 \text{ pc}}{D_L} \right) (1 - x) \right]^{\frac{1}{2}}, \quad (1)$$

where  $M_*$  is the mass of the lens and  $x = D_L/D_S$ . In the plane of the source lensed by VB 10, this angle subtends a distance larger than  $2000 R_\odot$ , assuming  $D_S = 1 \text{ kpc}$ . This suggests that finite-source-size effects are negligible, even if the substructures leading to planet-lens effects have sizes that are as small as 1% of the Einstein ring.

Several things are noteworthy about Equation 1. First, the value of  $\theta_E$  depends only on the lens mass and on  $D_L$  and  $D_S$ .  $D_L$  is potentially measurable for a nearby star; we have, for example, a high-precision measurement of the distance to VB 10. The value of  $D_S$  may not be known exactly, but the uncertainty in  $\sqrt{1 - x}$  is roughly  $x dx/2$  which can be small, since  $x$  is typically small. If, e.g., the distance to [VB 10]-PMLS-1 is a kpc, the uncertainty in  $\sqrt{1 - x}$  is approximately  $0.003 dx$ . If, therefore, we can measure the value of  $\theta_E$ , then we can measure the lens mass.

The value of  $\theta_E$  can be measured in two ways. The first is by fitting a lensing model to the light curve. A unique value of the magnification is associated with each value of the angular separation between the source and lens,  $u$ . If  $u$  is expressed in units of  $\theta_E$ , then the fractional magnification,  $A - 1$ , is roughly 0.34 for  $u = 1$ , 0.06 for  $u = 2$ , and 0.01 for  $u = 3.5$ . The magnification falls off as  $1/u^4$ . A lensing model fit allows us to derive the value of the Einstein diameter crossing time,  $\tau_E = 2 \theta_E / \mu$ , where  $\mu$  is the proper motion. The value of  $\mu$  can be measured for nearby stars, as it has been for VB 10. With  $\tau_E$  measured from the light curve, the value of  $\theta_E$  can be determined.

Second, lensing produces an astrometric shift in the position of the lensed source. The value of  $\theta_E$  can be measured by measuring the shift in the light centroid. The maximum value of the apparent shift in the source position occurs when the source and lens are separated by about  $\theta_E$ , and the size of the shift is roughly equal to  $\theta_E$ . The centroid shift

falls off as  $1/u$ . Thus, in the case of VB 10, the size of the Einstein angle is large enough that it can potentially be measured with high resolution images from *HST* or using adaptive optics from ground-based telescopes, such as Keck.

The duration of detectable lensing signatures can be significantly longer than  $\tau_E$ , which, for the VB 10 event is  $\sim 4.9$  days (the exact value is dependent on the proper motion of the background star). If magnification effects of  $\sim 6\%$  ( $\sim 1\%$ ) are detectable, then the duration of detectable deviations from baseline can be as long as  $\sim 10$  days ( $\sim 17$  days). The duration of detectable astrometric effects can be even longer, depending on the sensitivity of the measurements.

The detectability of both astrometric and photometric effects is complicated by the blending of light from the lensed source with light from other stars along the line of sight. In the case of lensing by VB 10, most of the additional light emanates from the lens itself. The source to be lensed, [VB 10]-PMLS-1, is a dim star. Because it is bluer than VB 10, changes in light from [VB 10]-PMLS-1 caused by VB 10 will be most detectable at shorter wavelengths. We have estimated the magnitudes of [VB 10]-PMLS-1 to be  $B \simeq 21.0$ ,  $I \simeq 18.2$  and  $H \simeq 16$  (Lépine & DiStefano 2011).

If the lens star is a binary, then the shape of the overall light curve, and the timing and magnitude of astrometric effects, will differ from the point-lens form. These deviations typically occur over a time scale that is comparable to  $\tau_E$ , and the value of  $\tau_E$  can still be derived from a lensing model fit.

If the lens star is orbited by planets, then a variety of signatures are possible. In the case of planets in orbits so wide that they essentially serve as independent lenses, their masses can be measured in the same way that the stellar mass can be measured. The time duration of the event will be shorter by a factor  $\sqrt{m_p/M_*}$ , where  $m_p$  is the mass of the planet. For closer orbital separations, the presence of the planet is signaled by a deviation from the point-lens event produced by the stellar lens. Model fits provide the mass ratio,  $q = m_p/M_*$ , so that the value of  $m_p$  can be expressed in terms of  $M_*$ . This paper is devoted to exploring the signatures of planets in predicted lensing events.

## 2.2. Predicted Paths and Approaches

The type of gravitational lensing effects that might be detectable, and their timing, depends on the paths of VB 10 and of the star to be lensed, [VB 10]-PMLS-1. Ideally we would be able to predict the exact path and compute the distance of closest approach to within a few mas, as well as the date of closest approach. Because, however, there are uncertainties in the position and speed of VB 10, and because we know little about [VB 10]-PMLS-1, an exact prediction is not yet possible. What we can do instead, is to construct an ensemble of paths, each consistent with all the available data.

We have run a Monte Carlo simulation that generates  $10^5$  possible paths. Six of them are shown in Figure 1, each with a different approximate angle of closest approach,  $b$ : 5 mas, 10 mas, 20 mas, 50 mas, 100 mas, and 150 mas. Table 1 lists the probability that the actual angle of closest approach,  $b$ , will be smaller than or equal to a given value,  $\phi$ . The table also lists the times of closest approach for the specific paths shown in Figure 1. We find that the times of closest approach range over several months during the end of

2011 and the beginning of 2012. The histogram in Figure 2 shows the distribution of event times. Note that, even if the closest approach occurs in winter 2011, planets can produce effects later in the winter or in the early spring, making them easier to observe.

### 2.3. Motivation: Does VB 10 have planets?

Several searches for planets around VB 10 have been conducted. A planet of  $\sim 6.4$  Jupiter-masses ( $M_J$ ) and a period of  $\sim 0.744$  yr (about 271 days) was proposed to have been the first around any star to be discovered by astrometry (Pravdo & Shaklan 2009). Pravdo and Shaklan fitted the observed data with a parallax and proper motion (PPM) model, and found that the probability of this describing the motion with no additional perturbations was very low. A PPM model combined with a Keplerian two-body model with the parameters above fitted the observed data well and thus the planet discovery was announced. One group tentatively confirmed this result, finding infra-red radial velocities consistent with Pravdo & Shaklan, but emphasizing the need for more measurements and better sampling to place absolute limits on parameters (Zapatero Osorio et al. 2009). Subsequent papers have ruled out the  $6.4M_J$ , 271-day planet, with various limits being placed on the possible parameters of any planets that may orbit VB 10 (Anglada-Escude et al. 2010; Bean et al. 2010; Lazorenko et al. 2011). Lazorenko et al. rule out the existence of  $6.4M_J$  and  $3.2M_J$  planets on the 271-day orbit with low false alarm probabilities using astrometry, and Anglada-Escude et al. place an upper limit of  $m \sin i \sim 2.5M_J$  using radial velocity (RV) measurements. Using high precision RVs, Bean et al. rule out masses greater than  $3M_J$ , and note that planets down to one Jupiter mass would have to have unusually large eccentricities ( $> 0.7$ ) to elude detection. Bean et al. also note that their higher precision measurements fail to confirm the Zapatero Osorio et al. result.

These limits do not rule out the possibility that VB 10 has planets. It would indeed be interesting to discover whether or not this star, with an estimated mass as low as generally considered compatible with core nuclear burning, harbors a system of planets. There is no *a priori* reason why it should not have planets, and evidence has been accumulating that low-mass stars can hold planetary retinues. Indeed the  $0.3M_{Sun}$  M dwarf GJ 581 is now the system with the largest number of confirmed planets (Mayor et al. 2010), and several

$\phi(mas)$	$P(b \leq \phi)(\%)$	date of closest approach for that path
5	2.5	15 Jan 2012
10	4.9	5 Feb 2012
20	9.4	14 Jan 2012
50	22.6	20 Jan 2012
100	43.7	17 Jan 2012
150	62.7	1 Feb 2012

Table 1: Column 1: angular separation,  $\phi$ , measured in mas. Column 2: probability that the angle of closest approach,  $b$ , between VB 10 and [VB 10]-PMLS-1 will be smaller than  $\phi$ . Column 3: the date of closest approach for the specific path shown in Figure 1, with angle of closest approach approximately equal to  $\phi$ .



other low-mass M dwarfs have been found to have planetary companions. A massive planet was also recently discovered orbiting an M dwarf through study of a lensing event (Batista et al. 2011).

Lensing observations complement observations of other types. For example, like astrometry, but unlike transit searches and radial velocity searches, lensing can identify planets in orbits with any orientation, including face-on. In addition, monitoring for lensing by a planet or planets orbiting VB 10, a star whose distance and spatial motion are well measured, would allow us to measure the gravitational mass of each planet discovered.

The predicted VB 10 lensing event presents a unique opportunity to probe for planets using mesolensing. We will either discover planets or place additional limits on their possible parameters. We have therefore considered planets in a wide range of orbits and with the following set of masses:  $3 M_J$ ,  $M_J$ ,  $M_{Saturn}$ ,  $M_{Neptune}$ ,  $M_{SEarth}$ . The symbol  $M_{SEarth}$  stands for the mass of a “SuperEarth”, which we have taken to be five times the mass of the Earth. We have modeled the proposed 271-day orbit as well as shorter and longer orbital periods.

## 2.4. Setting Scales

In Figure 1 we show paths that have distances of closest approach ranging from less than  $\theta_E$  to more than  $15 \theta_E$  (there is a 37.3% chance of having  $\beta > 15$  where  $\beta = b/\theta_E$ ). VB 10 would induce a magnification of (2.18, 1.34, 1.06) for distances of closest approach of (5 mas, 10 mas, 20 mas), respectively. Thus, the three paths shown which allow VB 10 to make approaches like these, could each allow VB 10 itself to produce a detectable magnification of the background star during a short interval of time near the point of closest approach. With a proper motion of  $1.5'' \text{ yr}^{-1}$ , it takes the system about 2.4 days to travel a distance equal to an Einstein radius,  $R_E$ . If a magnification of 1% is detectable, then the event could last as long as about 17 days.

This raises the exciting possibility that monitoring the region containing VB 10 several times per night during the month prior to and after the closest passage, will allow the first-ever detection of a predicted event [For a history of event prediction see DiStefano 2008a, and Paper II]. The mass of VB 10 could be determined to high precision.

The presence of planets around VB 10 can increase the magnification during the time of the stellar-lens event, making it more detectable. Planets can also produce events at much earlier or later times. Thus, even if the closest passage between VB 10 and the background star occurs when VB 10 is close to the Sun, planets can potentially produce events during the following months.

An important point to consider is that, although we cannot presently say exactly when the closest passage between VB 10 and [VB 10]-PMLS-1 will occur, it will be possible to conduct observations during 2012 that will allow us to determine the exact date on which it occurred and the minimum value of their angular separation. Once that is accomplished, every day during which VB 10 was observed one or more times will translate into a probability that the star hosts a planet with a given value of the projected orbital separation.

## 2.5. The Effects of Planets in three “Regimes”

To examine the photometric signatures of planets we have simulated lensing light curves produced by planetary systems. To derive the light curves we used a well tested code which computes the magnification for a binary lens with any combination of relative positions or masses. In the interest of speed, we have considered only circular face-on orbits, which allow us to delineate the key effects. In future work we will explicitly consider a more complete range of possible orbits. The type of lensing signature produced depends the lensing “regime” associated with each event.

There are two important distance scales, and they describe similar but separate entities. It is therefore important to define each clearly. The first scale refers to the distance between the lens star and its planets. If  $a$  is the instantaneous projected separation between VB 10 and a specific planet it may harbor, then  $\alpha = a/R_E$  is the quantity that determines the types of light curve features that can provide evidence that the planet exists. A close-orbit planet has  $\alpha < 0.5$ . A planet in the zone for resonant lensing has  $0.5 \leq \alpha < 2$ . A wide orbit planet has  $\alpha > 2$ . The value of  $\alpha$  determines the types of planet-lens signatures produced.

The second distance scale describes the distance of closest approach,  $\beta$ . The value of  $\beta$  determines which type of planetary orbit can produce detectable effects. A “regime” is defined by the range of values of  $\beta$  for which each type of planet-lens signature can be detected. In the “resonant regime” the effects of planets in the zone for resonant lensing can be detected; the value of  $\beta$  must generally be smaller than 2. In the “close regime” the effects of close-orbit planets are detectable. The close orbit regime extends from  $\beta = 0$  to an outer limit of  $2 - 10$ , depending on the sensitivity of the observations. The “wide-orbit regime” is defined by values of  $\beta$  for which the effects of wide-orbit planets are detectable. Like the other two regimes, it extends from  $\beta = 0$ , but the outer boundary is simply defined by the largest orbit possible. These definitions are summarized in Table 2. We note that the boundaries between the “close”, “resonant” and “wide” regimes are fuzzy, in the sense that there are generally not abrupt change in the signatures at specific values of the projected orbital separation, and that the location and size of the region over which the changes occur depend somewhat on the mass ratio,  $q$ . Nevertheless, there are significant differences that we will delineate in Sections 3, 4, and 5. The result is a rich set of signatures that can be used to explore the planetary system of VB 10.

Regime	$\beta$	$\alpha$	Light Curve
Resonant	$\lesssim 2.0$	$0.5 - 2.0$	Figure 3
Close	$\lesssim 5.0$	$\lesssim 0.5$	Figure 4
Wide	<i>all</i>	$\gtrsim 2.0$	Figure 5

Table 2: A summary of the properties of the three different regimes outlined in §2.5.1.  $\alpha$  is the orbital separation in units of  $\theta_E$  and  $\beta$  is the distance of closest approach in units of  $\theta_E$ .



### 2.5.1. “Resonant” Regime

Planets can produce different lensing effects depending on the projected orbital separation between the planet and star. Microlensing searches for planets have concentrated on planets in the so-called “zone for resonant lensing”, an annulus that extends from roughly  $0.5 R_E$  to approximately  $2 R_E$  ( $0.5 \lesssim \alpha \lesssim 2$ ). For planets located in this zone, the caustic structures associated with lens multiplicity are relatively large. When the path of the source brings it behind one of these structures, or even near to one, the magnification can be much larger than it would be otherwise. The light curve takes on a distinctive shape that signals the presence of the planet. In order for the path to allow the source star to come close enough to the caustics, we must be in the “resonant” regime,  $\beta \lesssim 2$ .

Several light curves produced by planets in the “zone for resonant lensing” are shown in both the top and bottom panels of Figure 3. In each case, the thick green solid curve shows the magnification expected if VB 10 does not have planets. Each of the other colors and line types corresponds to a light curve produced if VB 10 has a planet in the zone for resonant lensing. We will discuss this figure in more detail in §5. For now, the important features to notice are the high peak magnifications ( $> 3$  in most cases) exhibited by a large fraction of these light curves. Model fits can provide the values of the mass ratio and the projected orbital separation (in units of  $R_E$ ). In the case of VB 10, the zone for resonant lensing covers the angular range from 5 mas to 20 mas. The source would have to pass within this range in order for light curves like these to be produced. Thus, if the path of the source brings it within the inner circle shown in Figure 1, planets in the zone for resonant lensing could be discovered. For larger values of  $\beta$ , fewer such light curves occur. Once  $\beta \gtrsim 2$  they are rare. Hence we define the outer boundary of the resonant regime to be at  $\beta \approx 2$ .

### 2.5.2. Close-Orbit Regime

For values of  $\alpha$  less than roughly 0.5, the caustic structures are small, reducing the probability of detecting planets in close orbits. Furthermore, in ordinary microlensing, when the distance to the lens,  $D_L$  is typically only a few times smaller than the distance to the source,  $D_S$ ,  $\theta_E$  tends to be small, and finite-source-size effects can diminish the detectability of short-lived planet-induced deviations, further reducing the probability of planet detection.

For nearby lenses, however, it is possible to detect close-orbit planets (DiStefano 2011), and to determine the values of both  $q$  and  $\alpha$ . Not only are finite-source-size effects less important, but for nearby planets, the Einstein radius,  $R_E$ , is smaller, so that orbits with small values of  $\alpha$  are likely to have short orbital periods. The region in the lens plane with magnification deviations from the point-lens form can pass over the source star more than once. The repetition of deviations makes them more likely to be detected.

Light curves for some close-orbit planets are shown in Figure 4. Plotted is the difference between the magnification expected if there is a planet and the magnification expected if VB 10 alone passes in front of the source. Shown are light curves produced for a range of systems, which will be discussed in more detail in §4. For now, the important features to observe are the small size of the deviations and their repetitive nature. If ongoing or

repetitive deviations of a few percent are detectable, then Figure 4 illustrates that close-orbit planets with masses comparable to Saturn or Jupiter can be detected for  $\alpha$  as small as 0.3. For a given value of  $\alpha$ , the signatures are longer-lived for larger values of  $q$ .

By the “close-orbit regime” we mean the range of angles of closest approach for which the effects of close-orbit planets are detectable. The effects of close-orbit planets are detectable for very close approaches, but they are also detectable out to distances of  $\left(\frac{1}{\alpha} - \alpha\right)$ . For  $\alpha \sim 0.2$ , for example, the effects of close-orbit planets can be detected out to roughly  $5 R_E$ , 50 mas in the case of VB 10. Thus, close-orbit planets can be detected even if the distance of closest approach,  $\beta$ , is too large to detect planets in the zone for resonant lensing. The close-orbit regime extends from the origin to the edge of the disk with blue dots shown in Figure 1.

### 2.5.3. Wide-Orbit Regime

For larger distances of closest approach, the only planets that can be detected are those in wide orbits (DiStefano & Scalzo 1999a, 1999b). We will call a planetary orbit wide if its projected distance from VB 10 places it outside of the zone for resonant lensing ( $\alpha$  greater than about 2). The presence of wide-orbit planets can be inferred in one of two ways. First, the presence of the planet can cause alterations in both the position of the stellar lens and in the isomagnification contours around the stellar lens. Examination of the light curve produced by the star can therefore reveal the presence of wide-orbit planets. Second, the planet itself may pass close to the background star [VB 10]-PMLS-1, even though VB 10 itself does not.

For wide separations, the planet may essentially serve as an independent lens, producing a lensing light curve likely to be similar to one that would be produced by an isolated lens. Figure 5 shows a sequence of events in which the value of  $\alpha$  ranges from 2 to 20. In each case, there is a red light curve and a blue light curve corresponding to clockwise and counterclockwise face-on circular orbits, respectively. The time between the short-lived planet-induced deviation and the time of the peak of the stellar-lens event becomes progressively longer as  $\alpha$  increases, and the durations more closely mirror what they would have been without VB 10. Note that we have plotted each column with one range of times, but the range changes from column to column in order to optimize the presentation. We will consider these light curves further, and derive some of the relevant properties in §3.

## 3. Wide-Orbit Regime

### 3.1. Wide Orbits and the advantages they confer

Wide-orbit planets would be so far from VB 10 that they can produce a separate event in the days, weeks, months or even years prior to or after the closest passage between VB 10 and the background star. Thus, if VB 10 hosts planets in wide orbits, the events they produce could occur at times when variations in [VB 10]-PMLS-1 are easier to detect, even if the closest passage between VB 10 and [VB 10]-PMLS-1 occurs when the Sun’s position is not favorable for the detection of the stellar-lens event. In addition to the advantage

provided by a delayed event time, the event produced by a wide-orbit planet may happen to produce a larger magnification of [VB 10]-PMLS-1 than VB 10 itself ever does.

It would be difficult to specify a unique value of the projected separation,  $\alpha$ , above which an orbit should be considered “wide”. If a planet and star have a projected orbital separation of approximately an Einstein radius, the isomagnification contours are not asymmetric, and many corresponding to detectable magnifications encompass both star and planet. As the planet is moved farther from the star, the isomagnification contours separate and, for large enough orbits, the pattern of contours around the planet and star are each similar to the pattern expected for isolated masses (Figure 6). Light curves which show simultaneous evidence of lensing by both the star and planet become rarer as the projected separation increases.

The star and planet can each produce well-separated events for projected separations as small as  $1.5 \theta_E$ , although this result depends on the value of the mass ratio and on the photometric sensitivity of the observations. In this paper, we consider the inner boundary of the wide regime to be approximately  $2 \theta_E$ . It is important to note, however, that, even though the planet-lens event may be separate from the stellar-lens event, the shape of the light curve associated with lensing by the planet can be influenced by the presence of the star until the value of  $\alpha$  is fairly large: Figure 6 shows that the 1% isomagnification contour is significantly distorted from a circular form, even for  $\alpha \sim 6$ . The significance of these distortions is twofold: they influence the light curve characteristics and, because they increase the linear dimensions of the region within which the magnification is significant, they increase the event probability.

Interestingly enough, in the case of VB 10, its well-studied spatial motion allows us to determine a maximum orbital separation for a planet of a given mass. If VB 10 has a planet of mass  $m_p$ , with a maximum separation from the center of mass of  $a_{max}$ , then VB 10 has a maximum separation  $a_*$  from the center of mass of  $a_* = a m_p / M_*$ . There are, however, limits on the value of  $a_*$  which can be derived from the astrometric limits of Lazorenko et al. (2011). Specifically, if a planet of  $6 M_J$  in a 271 day orbit is ruled out, then the maximum separation between VB 10 and the center of mass is  $\delta_* \sim 5 mas$ . Taking this as a rough guideline, the maximum orbital separation of the planet can be expressed as follows.

$$a_{max} \sim 2.18 AU \frac{\delta_*}{5 mas} \left( \frac{M_*}{0.075 M_\odot} \right) \left( \frac{0.001 M_\odot}{m_p} \right) \quad (2)$$

At the distance to VB 10, this corresponds to a maximum angular separation between a Jupiter-mass planet and VB 10 of about  $0.38'' = 38 \theta_E$ . For less massive planets, wide planets may have proportionally larger orbits.

### 3.2. Relationship between orbital parameters and event properties

The effects of parallax introduce significant deviations from straight-line motion. Nevertheless, it is possible to use the straight-line approximation to estimate the relationship between the properties of a planetary orbit and the time at which an event caused by the planet will occur. Let  $t_0$  be the time of closest passage between VB 10 and the background

star, and let  $\beta$  be the distance of closest approach expressed in units of  $\theta_E$ . If the time is expressed in days, and the proper motion  $\mu$  is expressed in units of  $\theta_E/\text{day}$ , then

$$\left| t - t_0 \right| = 2.5 \text{ days} \left( \frac{0.4 \frac{\theta_E}{\text{day}}}{\mu} \right) \left( \alpha^2 - \beta^2 \right)^{\frac{1}{2}} \quad (3)$$

In order for the planet to create an independent event, it must generally be farther from VB 10 than the closest approach to the background star ( $\alpha > \beta$ ). For a given path,  $\beta$  has a fixed value. Suppose the value of  $\beta$  happens to be large: for example,  $\beta = 10$ . Then orbits with values of  $\alpha$  near 10 could produce detectable effects close to the time of closest approach, should the orbital phase happen to be just right. Whatever the value of  $\beta$ , small or large, planets in orbits with progressively larger values of  $\alpha$  can produce events at longer time intervals before or after the closest passage.

Equation 3 highlights an important feature of predicted events, or indeed any event in which the angle of closest approach is known. *During any given day before or after the event, we can compute the specific value of  $\alpha$ , the projected orbital separation, of the planet whose lensing signature we can detect on that day.* Actually, we compute a small range of possible values of  $\alpha$ , since the size of the lensing region around the planet has a finite extent which can be computed for each set of values of  $q$  and  $\alpha$  (See Figure 6.) Uncertainties in the path also produce uncertainties in the possible day-by-day values of  $\alpha$ . Thus, if an event is detected on a specific day, say the 30th day after the main event, we can immediately estimate the value of  $\alpha$  (Figure 7). The features of the associated light curve, including the value of  $\tau_E$ , allow us to estimate the mass of the planet, if the proper motion can be estimated.

Conversely, if no detection is made on a given day, we know what type of orbit is *not* producing an event. Lack of evidence for an event on any given day does not translate to evidence for lack of a planet. It does, however, allow us to place limits on the possible presence of a planet as follows. We consider the times the observations that have been made and, for each, the minimum value of the magnification to which the observation would have been sensitive. Then, by generating a large number of orbits for each value of  $\alpha$  and each value of  $q$ , including a range of orbital eccentricities and inclinations, we can compute what fraction of the time a planet of each type would be detected. If the observations would have detected the planet 100% of the time, then the failure to observe the planet means that it is not there. If, however, the probability of detecting the planet is  $\mathcal{P}$ , then we can say that there is now a probability of only  $1 - \mathcal{P}$  that such a planet orbits the lens star.

The top panel of Figure 7 shows the relationship between  $\alpha$  and  $|t - t_0|$ , predicted by Equation 3. That this relationship is approximately correct is verified by the positions of the hexagons (for clockwise orbits) and filled crosses (for counterclockwise orbits), corresponding to systems included in our simulations for the 5 mas approach (red curve). The analytic results for the other 5 approaches are also shown. The middle panel shows the orbital period for each of the 6 approaches. The bottom panel shows the analytic relationship between the ratio of the orbital speed to proper motion as a function of  $\alpha$ . The significance of this last panel is that it allows us to estimate the effect that orbital motion may have on the duration of wide-orbit planet-lens events. This panel shows that, for

values of  $\alpha$  that produce deviations at times longer than 10 – 20 days prior to or after the closest approach, the effects of orbital motion become negligible, but that orbital motion can influence the light curves for values of  $\alpha$  that produce planet-lens effects closer to  $t_0$ . This is consistent with, for example, the longer duration of planet-lens events for clockwise versus counterclockwise orbits shown for  $\alpha$  smaller than about 7 in Figure 5.

**Note on the time scales:** The angular speed of VB 10 is high, and the mass of the star is very low. This combination means that the Einstein-diameter crossing time is smaller than typical, even for nearby stars. A star of mass equal to  $0.5 M_\odot$  located 50 pc away and lensing a distant source would have the same value of  $\theta_E$  as VB 10, but would have an angular speed likely to be only a tenth as large. This means that the time scales on the horizontal axis of Figure 7 would be multiplied by a factor of about 10. Thus, for example, planets with  $\alpha = 20$  could cause events 500 days prior to or after the time of closest approach. In addition, events would last longer, making isolated planet-lens events easier to detect. Furthermore, orbital motion is more likely to be significant, rotating perturbed isomagnification contours into the vicinity of the background source, thereby increasing the event probability. We will return to this question in Paper II when we consider predicted events that are more ideal for detection than the predicted VB 10 event.

### 3.3. Event Probabilities

To estimate the probability that a wide-orbit planet will produce an event, we have conducted sets of simulations. In each simulation, the center of mass follows one of the six paths shown in Figure 1, and VB 10 is orbited by a planet of fixed mass,  $m_p$ , which executes a face-on circular orbit (either clockwise or counterclockwise) with a specific value of  $\alpha$ . The simulation consists of generating a number of light curves (up to 50,000), differing from each other because the initial orbital phase is chosen from a uniform random distribution. By computing the fraction of the generated events that display a specific event characteristic, we determine the probability that that characteristic will occur, should a planet of mass  $m_p$  inhabit that type of orbit. [Note that the orbit is defined as a face-on circular orbit with a specific value of  $\alpha$  and a specific orientation (clockwise or counterclockwise).]

Results are shown in Figures 8 and 9. Plotted in Figure 8 is the maximum difference between the planet-lens light curve and the light curve generated by VB 10 alone, as a function of initial orbital phase. The sharp peaks correspond to cases in which the planet generated a clear independent event. The probability that a planet-induced event with a peak magnification above a certain value can be computed by finding the fraction of phases in which the magnification achieves this value or an even larger one. The results are shown in Figure 9. For close approaches and modest values of  $\alpha$ , the probability of a planet-induced deviation larger than a few percent can be larger than 0.1. For more distant approaches, only planets with wider orbits can produce events, and the probability is corresponding lower, on the order of 1%. Analogous calculations apply to planets of smaller mass, which can be located even farther from VB 10 without inducing motion in VB 10 that would have already been detected by, e.g., Pravdo & Shaklan (2009) or other astrometric studies.

A simple analytic approach to computing the probability that a wide-orbit planet will

produce a separate short-duration event is to compare the size of the region within which a planet produces significant effects with the size of the orbit. This ignores velocity effects, but can nevertheless provide a reasonable estimate of the fraction,  $P$ , of initial phases likely to produce an isolated planet-lens event.

To compute this fraction, we simply need to compute the ratio between (1) the size of the region around the planet that can produce detectable lensing effects, and, (2) the size of the orbit. We will express each in units of the Einstein radius. The denominator, the size of the orbit, is simply  $2\pi\alpha$ . Developing a good approximation for the value of the numerator requires some care. First, the size of the region within which lensing can be detected depends on the sensitivity of the observations. If only magnifications of 34% (6%, 1%) or more are detectable, then the width of the lensing region is  $1 \times (2R_E)$  [ $2 \times (2R_E)$ ,  $3.5 \times (2R_E)$ ]. The factor to the left in each case correspond to the distance, in Einstein radii, at which the magnification becomes detectable. We have taken this into account by introducing a factor  $F/2$ , which is unity when deviations of 6% are detectable, 0.5 if deviations must be larger than 34% are detectable,  $3.5/2 = 1.75$  if deviations must be larger than 1% to be detectable.

A second factor influences the size of the lensing region associated with the planet. This is the proximity of the star. For values of  $\alpha$  in the range  $2 - 6$ , the lensing region is significantly stretched, with the amount of stretching also dependent on the mass ratio,  $q$ . For larger values of  $\alpha$  the stretching is minimal. To take this into account, we have introduced the factor  $E(q_i, \alpha)/1.5$ , which has the value roughly equal to 1 for  $\alpha = 3$  and  $q = 0.001$ .

With these definitions, the probability,  $P$ , that a wide-orbit planet will produce an isolated event is

$$P = 0.36 \frac{F}{2} \sum_{i=1}^n \left( \frac{q_i}{0.01} \right)^{\frac{1}{2}} \left( \frac{1}{\alpha_i} \right) \left( \frac{E(q_i, \alpha_i)}{1.5} \right), \quad (4)$$

where the sum is over wide-orbit planets. For  $\alpha = 3$ , the contribution is 0.12, in line with the results shown in the graphs. We consider a sum over possible planets to include the possibility that VB 10 has multiple wide-orbit planets. Note that the peak in the probability distribution for  $\alpha$  larger than unity, that has declined significantly in all cases before  $\alpha = 10$ , corresponds to the decreasing probability that the wide-orbit planet will produce its own isolated event as  $\alpha$  increases.

### 3.4. Detecting evidence of the planet during the stellar-lens event

In Equation (2) we considered the size of the astrometric shift of the lens star associated with the planetary orbit. From the astrometric studies of VB 10 (see §2.3), we know that the shift is small ( $\lesssim 5$  mas). Given that  $\theta_E \sim 10$  mas, even a small shift can, however, change the magnification in a manner that is detectable. *Magnification effects can enhance the detectability of small shifts in the position of the star.*

Consider the following example. On the 5 mas approach, a shift in position of just 1 mas could cause the peak magnification to increase from  $A = 2.18$  to  $A = 2.64$ . A quick calculation finds that a 1 mas shift in the position of VB 10 could be caused by a Jupiter-mass planet in an orbit of  $\sim 0.44$  AU, a perfectly feasible possibility.



The light curves in Figure 5 show shifts in both the time and magnification of the stellar-lens event due to this effect. The probability associated of this effect being detectable is quantified in Figures 10 ( $\beta \sim 0.5$ ) and 11 ( $\beta \sim 1$ ) for large  $\alpha$ . Each of these two figures consists of panels, each for a single planet mass, ranging from a SuperEarth to a planet 3 times as massive as Jupiter. The light black curve shows the probability that a deviation 1% or larger will occur. Every subsequent curve corresponds to a deviation 2 times larger than the last. One obvious effect is that there is an increasing probability of deviations toward larger values of  $\alpha$ . This is seen in every panel of Figure 10, and for the  $3M_J$ ,  $M_J$ , and  $M_S$  panels of Figure 11. This corresponds to an increasing probability of stellar astrometric shifts producing detectable deviations from the point-lens light curve.

These results imply that fits to light curves produced by the star have the potential to identify deviations from the point-lens form and to discover wide-orbit planets. *This is the case even when the planet itself does not produce a separate detectable event.* Figures 10 and 11 demonstrate that the increase in detection probability is significant. Alternatively, if the planet does produce an independent event, then a check for consistency between information derived through the planet-lens and stellar-lens events can be made.

## 4. Close Orbits

### 4.1. Close Orbits and the advantages they confer

If VB 10 happens to have planets with orbits much smaller than the Einstein radius, the lensing signatures can also be significantly perturbed. This is because there is a small region within which the isomagnification contours are distorted from the circular form they would have had in the absence of the planet. These perturbations are typically maximized at a distance  $R_\alpha = (\frac{1}{\alpha} - \alpha)$  from the center of mass.  $R_\alpha$  can be as large as several times  $\theta_E$  for  $\alpha \ll 1$ . In the absence of orbital motion, there would be only a small probability that the distorted region would pass in front of the source. The orbital period is short for small values of  $\alpha$ , however. For example, a face-on circular orbit with  $\alpha = 0.2$  would correspond to an orbital period around VB 10 of roughly 1.7 days. This means that there can be a good chance that the distorted region will rotate in front of the source star, possibly even more than once.

Thus, even though the deviations tend to be small, repetition confers an advantage. In Figure 4 light curves associated with close-orbit planets are shown. Plotted is  $A_{pl} - A_{pt}$ , where  $A_{pl}$  is the magnification of the planet-lens light curve and  $A_{pt}$  is the point-lens light curve that would be produced by VB 10 alone. While the individual deviations can be short-lived, the time interval over which they occur can be long, starting days before the closest approach and continuing until days after. The timescales could be much larger for other lens stars (see *Note on the Timescales*, §3.2 and Paper II).

Figure 4 shows that even a Saturn-mass planet can produce detectable ( $> 1\%$ ) effects for  $\alpha$  as small as 0.3. Because the size of the deviations is smaller for smaller  $\alpha$ , but the deviations are enhanced for more massive planets, we compare Jupiter-mass and Saturn-mass planets for  $\alpha = 0.3$ , and Jupiter-mass planets and 3-Jupiter-mass planets for  $\alpha = 0.2$ .

The effects we see at early and late times are caused by the isomagnification deviations at  $R_\alpha$ . The deviations seen near the time of closest approach are associated with the

astrometric motion of VB 10 itself, which is just a small wobble executed during the planet’s orbit. As is the case for wide-orbit planets, lensing enhances the effect of the wobble by changing the position of the lens at the time of closest approach (see §4.3)

Figure 12 also shows close-orbit light curves. Here, as in the third panel from the top in Figure 4, we show the results for a Jupiter-mass planet with  $\alpha = 0.2$ . Whereas in Figure 4, the angle of closest approach was  $\sim 5$  mas ( $\beta = 0.5$ ), the distances of closest approach are varied in Figure 12. We have  $\beta = 1, 2, 5$ , progressing from the top panel to the bottom panel. the larger the value of  $\beta$  the smaller the effects, and the more sensitive the photometry required for detection.

Just as there is a largest orbital separation for a wide-orbit planet, there is a smallest orbital separation for a close-orbit planet. To avoid catastrophic tidal disruption a planet must satisfy the condition  $r_h \gtrsim 2r_p$ , where  $r_h$  is the Hill radius given by  $r_h \approx a(\frac{m_p}{3M_*})^{1/3}$ . Thus the minimum orbital separation of a planet around VB 10 is roughly given by

$$a_{min} \sim 0.3R_\odot \frac{r_p}{r_J} \left( \frac{M_*}{0.075M_\odot} \right)^{1/3} \left( \frac{0.001M_\odot}{m_p} \right)^{1/3} \quad (5)$$

This corresponds to  $\alpha_{min} \sim 0.03$  for the VB 10 case.

#### 4.2. Relationship between orbital parameters and event properties

Close-orbit planets produce deviations both in advance of and after the closest approach. The time at which the deviations start is the time at which the region at  $R_\alpha$  passes in front of the source star. Let  $t_{max}$  be the time at which deviations related to the planet begin or end, representing the maximum time difference between the time of closest approach and the time at which deviations occur. If we measure time in days we have the analogue to Equation (3) for close-orbit planets:

$$\left| t_{max} - t_0 \right| \sim 2.5 \left( \frac{0.4 \frac{\theta_E}{\text{day}}}{\mu} \right) \left( \left( \frac{1}{\alpha} - \alpha \right)^2 - \beta^2 \right)^{\frac{1}{2}} \quad (6)$$

In this case, the smaller the value of  $\alpha$ , the longer the difference in time between the stellar-lens event and the planet-lens event. This effect is shown in Figures 4 and 12.

As in §3.2, we can compute a specific value of  $\alpha$  for a planet whose lensing signature we are capable of detecting on a given day. The top panel of Figure 13 shows the relation between  $\alpha$  and  $|t_{max} - t_0|$  predicted by Equation (6) and is analogous to Figure 7 for wide orbits. Figure 13 also shows the important role of orbital motion in the close regime: The orbital period decreases with decreasing  $\alpha$ , corresponding to larger values of  $|t_{max} - t_0|$  (middle panel). As the orbital period decreases, the ratio of orbital velocity and proper motion,  $v_{orb}/\mu$ , increases, and plays an important role in the lensing signatures (Guo et al. 2011, Penny et al. 2011, DiStefano 2011). The relationship between  $v_{orb}/\mu$  and  $|t_{max} - t_0|$  is shown in the bottom panel of Figure 13.

Note that there is an overlap between the region in which the effects of wide-orbit and close-orbit planets can be detected. If, for example, the distance of closest approach is  $3\theta_E$ , then at similar times before and after the “main” event, it would be possible to

detect both a wide-orbit planet with  $\alpha$  in the range  $5 - 6$  and a close-orbit planet with  $\alpha$  in the range  $0.15 - 0.2$ . Of course planets in wider orbits could also be detected at much earlier and much later times. The details of the close regime are presented in DiStefano (2011).

### 4.3. Event Probabilities

The detection of close orbit planets relies on being sensitive to small deviations, on the order of a few percent or smaller, each of which may last less than a day. Repetition means that, even if a deviation is missed, however, there still are other opportunities to establish with high reliability, the occurrence of ongoing deviations.

Consider the case of a close-orbit planet orbiting VB 10 with  $\alpha = 0.3$ . The orbital period is approximately 3 days, producing deviations that repeat on a three day time scale, with the largest deviations occurring when the distance between the source and lens is approximately  $3\theta_E$ , when the average magnification is about  $(1 - 2)\%$ . As Figure 4 shows, the deviations can be larger than a percent.

In Figures 4 and 12, each panel contains 9 independent light curves, slightly displaced from each other so that the variations in each can be resolved. The nine light curves in each panel differ from each other only in that a different initial phase was chosen for each. *The effects were similar in all cases.* This demonstrates that, if the observational strategy is capable of detecting deviations caused by planets with a given value of  $\alpha$ , orbital period, and  $q$ , then it will detect such planets with certainty. Thus, limits on close orbit planets can always be placed, if the observing conditions are favorable and the monitoring program is well designed. the values of  $\alpha$  for which we can derive limits or else guarantee a detection are determined by the photometric sensitivity, whilst those of  $q$  are determined by the cadence of sampling.

### 4.4. Detecting evidence of the planet during the stellar-lens event

As a close-orbit planet orbits a star, the star wobbles in its own smaller orbit. When the star serves as a lens, small changes in its position can make a measurable difference in the magnification it produces in a background star. This effect is responsible for the deviations displayed near the time of closest approach in each of the light curves in Figure 4.

In units of the Einstein angle, the wobble of the star has amplitude

$$\delta = \frac{m_p}{M_J} \frac{\alpha}{0.3} \quad (7)$$

This leads to a magnitude variation  $(A(\beta - \delta) - A(\beta + \delta))$ , where  $\beta$  is the distance of closest approach in units of  $\theta_E$ . For  $\beta = 0.5$ , corresponding to the 5 mas approach, the variation is  $7.3\delta = 0.03$ . For  $\beta = 1$  corresponding to the 10 mas approach, the variation is  $1.4\delta = 0.006$ . As the distance of closest approach increases, the central deviations become smaller and are less easily detected. Nevertheless, there are clearly some cases in which the magnification deviations caused by the astrometric shifts of the central star provide the strongest signature of lensing.

## 5. Orbits in the Zone for Resonant Lensing

### 5.1. Orbits in the Zone for Resonant Lensing, and the advantages they confer

When the possibility for discovering planets via microlensing was first discussed (Mao & Paczyński 1991; Gould & Loeb 1992), attention focused on cases in which the projected orbital separation between star and planet lies in the range  $0.5 R_E - 1.5 R_E$ . For separations in this range, caustic curves play an important role and produce high magnifications. Ground-based microlensing searches for planets have focused on finding planets in this resonant zone. Lensing events are found by observing teams monitoring wide fields. Events judged to have a high probability of exhibiting large magnification are targeted for almost continuous monitoring during the interval when the magnification is high. Such intensive monitoring has a good chance of discovering planets in the resonant zone and, if there is no discovery, limits on their presence can be placed (Griest & Safizadeh 1998).

For VB 10, angular separations between  $0.5 \theta_E$  and  $1.5 \theta_E$  correspond to projected distances in the lens plane which are in the range 0.026 AU–0.079 AU ( $5.6 R_\odot - 17 R_\odot$ )<sup>1</sup>. Thus, the mean annular radius of the zone for resonant lensing is so small that the orbital period of any planets inhabiting this zone are short. For circular orbits, the periods range from about 6 days to roughly 33 days. Because it takes approximately 7 days for VB 10 to cross a distance of  $3 \theta_E$ , comparable to the distance over which dramatic lensing events could be observed, the probability of seeing planet-induced lensing effects is high. In essence, the region in the lens plane in which the isomagnification curves are very perturbed from the point-lens form, rotate over the position of the distant source. As long as  $\beta$  is small enough that planets in the zone for resonant lensing produce detectable events, the probability of detection can be high.

### 5.2. Event Probabilities

The closer the approach, the higher the probability of detecting events in which the source has passed near a caustic structure. This is illustrated in Figure 3, where light curves for a 5 mas approach are shown. For  $\alpha = 1.2$  (top panel) and  $\alpha = 0.8$  (bottom panel), ten randomly selected initial phases were each used to generate a light curve. For  $\alpha = 1.2$ , eight of the light curves showed significant deviations, three involving caustic crossings (those exhibiting wall-like rises and falls). For  $\alpha = 0.8$ , all ten light curves displayed significant variations, with an even larger number of caustic crossings than for  $\alpha = 1.2$ .

Figure 14 shows the probabilities and timescales associated with caustic crossings as a function of  $\alpha$ , for both 5 mas and 10 mas approaches, and both clockwise and counter-clockwise orbits. Multiple light curves were computed, and whenever a caustic crossing occurred, the characteristics of the event were noted. As we would expect, the probabilities and crossing times are markedly higher for the closest approach. There is also a significant

---

<sup>1</sup>As pointed out in §2.1, in mesolensing events, the source plane is far enough away that finite source-size effects are not expected to be problematic.

difference in behavior for clockwise (blue) and counter clockwise (red) orbits. Clockwise orbits tend to produce longer events, but the probability of a caustic crossing is somewhat reduced compared to the counterclockwise case. For  $\alpha = 1.5, \beta = 0.5$  in clockwise orbits,  $\sim 25\%$  of light curves exhibit caustic crossings with a typical timescale of  $\sim 6$  hours. This contrasts with  $\sim 45\%$  of light curves and timescales of  $\sim 3$  hours in the counter clockwise case.

Note, however, that caustic crossings are not needed to produce a large increase in magnification. This is shown by the presence of smooth curves in Figure 3, which do not exhibit the sharp features of a caustic crossing but which nevertheless produce detectable deviations. In Figures 10 and 11, the probability that deviations of a certain size will occur, starting at 1% and increasing by a factor of two in each subsequent curve (see §3.4) are shown. For the 5 mas ( $\beta = 0.5$ ) approach, the probability of deviations of a few percent is near unity for a Jupiter-mass planet, tens of percent for a Saturn-mass planet, and a few percent for a SuperEarth, these probabilities decline for larger values of  $\beta$ , as can be seen even in Figure 11, where  $\beta = 1$ .

## 6. Conclusions

The close approach between VB 10 and [VB 10]-PMLS-1 is not the ideal predicted mesolensing event; its distinction is in being the first. Here we have shown that, even with the uncertainties associated with the event, and the relative difficulties of observing the more subtle effects, it is possible to make a number of predictions about the types of events we may see and when we may see them. **(1)** We have shown that planets can be detected in three different orbital ranges, depending on the sensitivity of the observations and the exact characteristics of the approach. We have characterized the of lensing signatures that are produced in each orbital zone and distance regime. **(2)** We have shown that the time of the event relative to the time of closest approach depends on the orbital separation, and that on a given day there is a specific range of orbital separations for which planets can be detected.

This knowledge can be used to coordinate observing programs and probe for planets in a more systematic way than has been done so far. The method to be used is applicable to all high proper motion stars, and has a range of other applications which we explore in Paper II.

VB 10 has been observed by the MEarth and GROND projects, and future observations are planned in the coming months. While discovery, or the placing of limits, is possible in the case of VB 10, our program will also serve as a training ground for future observations. *In Paper II of this discussion we elaborate further on the specifics of VB 10, and on the possibility of observing predicted events in the more general case.*

## Acknowledgements

We would like to thank Christopher Stubbs; Christopher Crockett; Fred Walters; David Charbonneau, Zachory Berta and the MEarth project; Jochen Greiner at GROND; Matthew Templeton and the AAVSO for their help and advice with observing VB 10. This work was supported in part by NSF under AST-0908878.

## REFERENCES

- Anglada-Escude, et al. 2010, ApJ, 711, L24
- Batista, V., et al. 2011, A&A, 529, 102
- Bean, J. L., et al. 2010 ApJ, 711, L19
- Bolatto, A. D., & Falco, E. E., 1994, ApJ, 436, 112
- Di Stefano, R., 2008a, ApJ, 684, 46
- Di Stefano, R., 2008b, ApJ, 684, 59
- Di Stefano, R., 2011, ApJ submitted, arXiv:1112.2366v1
- Di Stefano, R., 2012, Paper II, ApJ submitted
- Di Stefano, R., & Night, C. 2008, arXiv:0801.1510
- Di Stefano, R., & Scalzo, R. A. 1999a, ApJ, 512, 564
- Di Stefano, R., & Scalzo, R. A. 1999b, ApJ, 512, 579
- Feibelman, W. A. 1966, Science 151, 73
- Feibelman, W. A. 1986, PASP98, 1199
- Guo, X., et al. 2011, arXiv:1112.4608G
- Gould, A., & Loeb, A. 1992, ApJ, 396, 104
- Greiner, J., et al. 2008 PASP, 120, 405
- Griest, K., & Safizadeh, N. 1998, ApJ, 500, 37
- Hilton, E. J., et al. 2010, AJ, 140, 1402
- Irwin, J., et al. 2008, arXiv:0807.1316v1
- Lazorenko, P. F., et al. 2011, A&A, 527, 25
- Lépine, S. & Di Stefano, R. 2011, ApJ submitted, arXiv:1111.5850
- Mao, S., & Paczynski, B. 1991, ApJ, 374, 37
- Mayor, M., et al. 2010, A&A, 507, 487
- Paczynski, B. 1995, Acta Astronomica, 45, 345
- Penny, M. T. et al. 2011, MNRAS417, 2216
- Pravdo, E., & Shaklan 2009, ApJ, 700, 623



Salim, S., & Gould, A. 2000, ApJ, 539, 241

Van Biesbroeck, G. 1944, AJ, 51, 61

West, A. A., et al. 2008, ApJ, 135, 785

Zapatero Osorio, M. R. et al. 2009, A&A, 505, L5

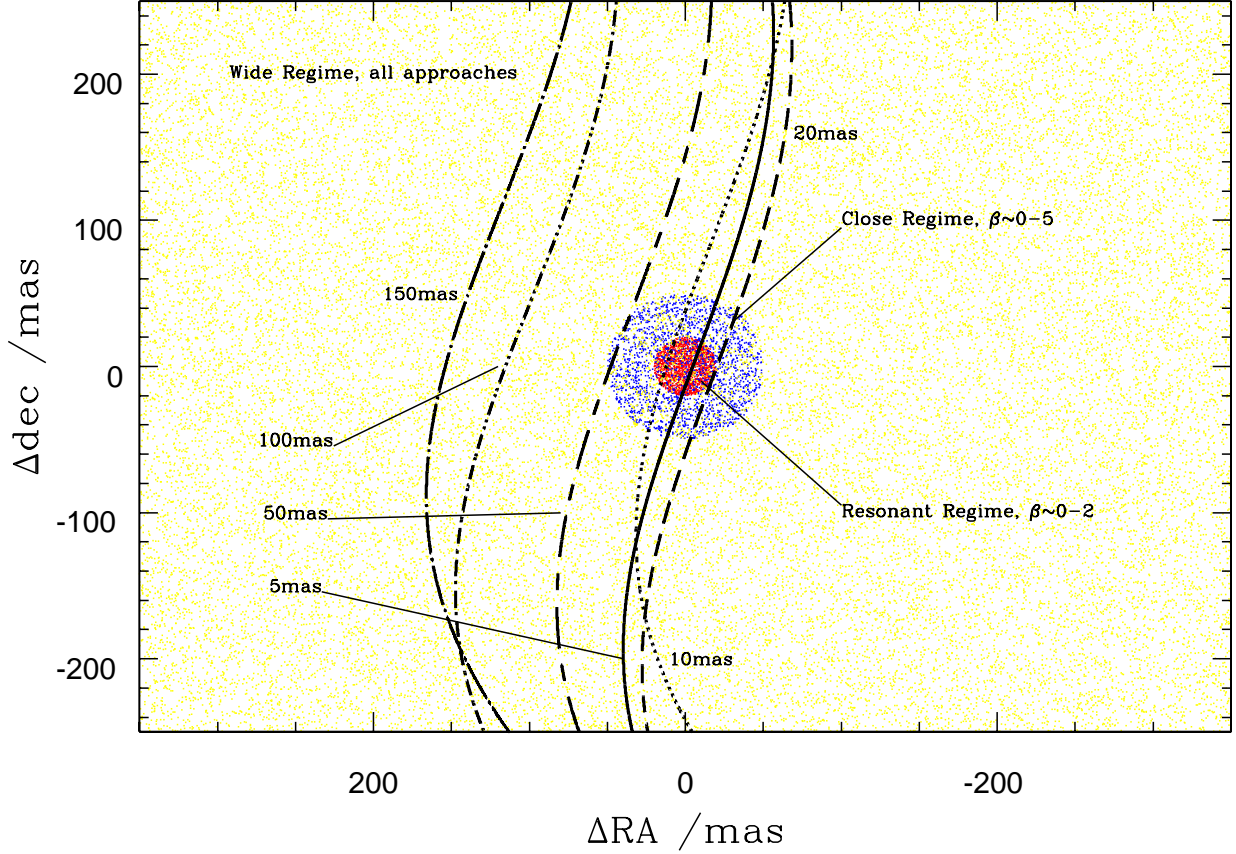


Fig. 1.— Six possible paths of VB 10 where  $(\Delta\text{RA}, \Delta\text{dec})$  is the position in mas relative to the background star at the origin. The approximate angular distance of closest approach for each path is labeled, and the sinusoidal type shape of the paths is due to parallax. Each of the three background colors corresponds to a region around the background star in which planets can be detected. If the distance of closest approach is inside the yellow zone (from the origin outwards) then we are in the *wide regime*, and can detect wide-orbit planets. If the distance of closest approach is inside the *close regime* (blue,  $\beta \lesssim 5$ ), and small deviations from baseline can be detected, then we can discover evidence of close-orbit planets. If the distance of closest approach is inside the innermost red region then we are in the *resonant regime* ( $\beta \lesssim 2$ ) and can detect standard planet-lens effects such as caustic crossings.

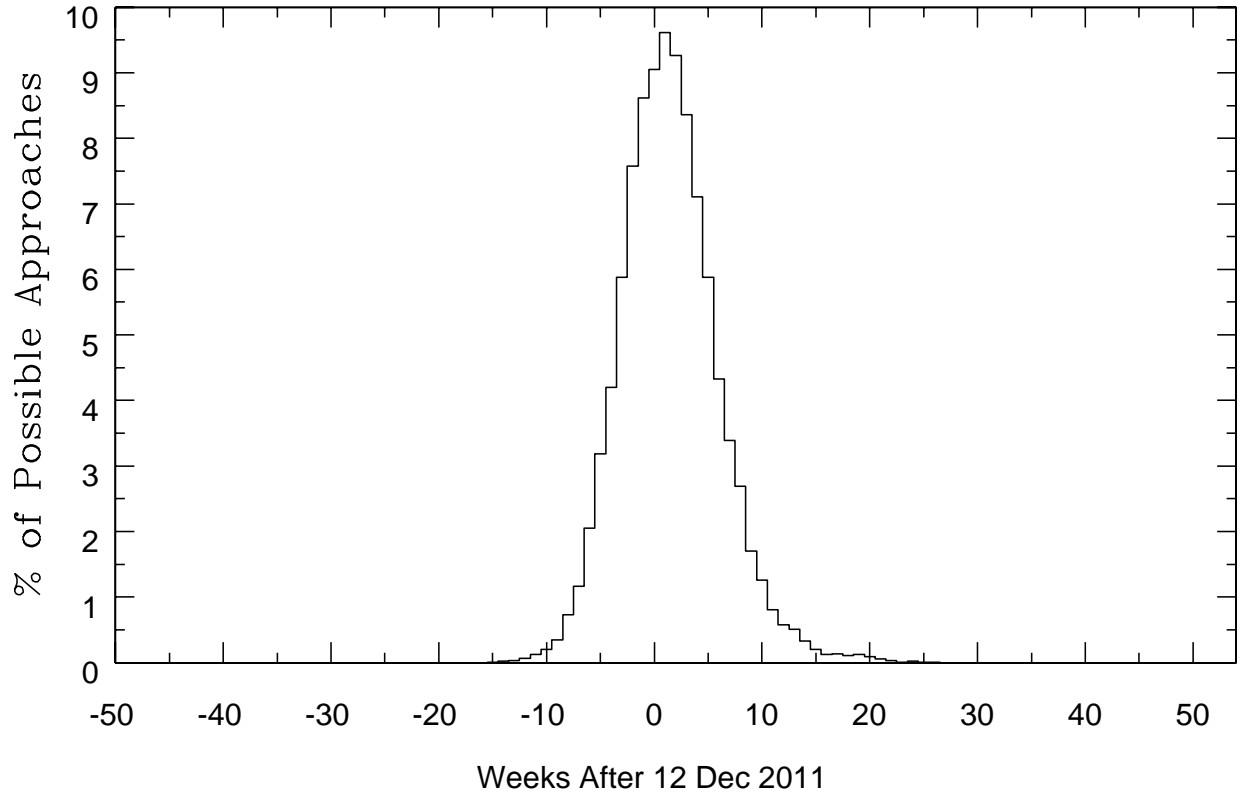


Fig. 2.— Probability distribution for the time of closest approach, derived from Monte Carlo simulations accounting for uncertainties in the astrometric motion of VB 10 relative to the background star. The data are binned according to week, with the most likely time being during the week beginning 19th December 2011. However, there is a chance that the event will occur as late as May 2012.

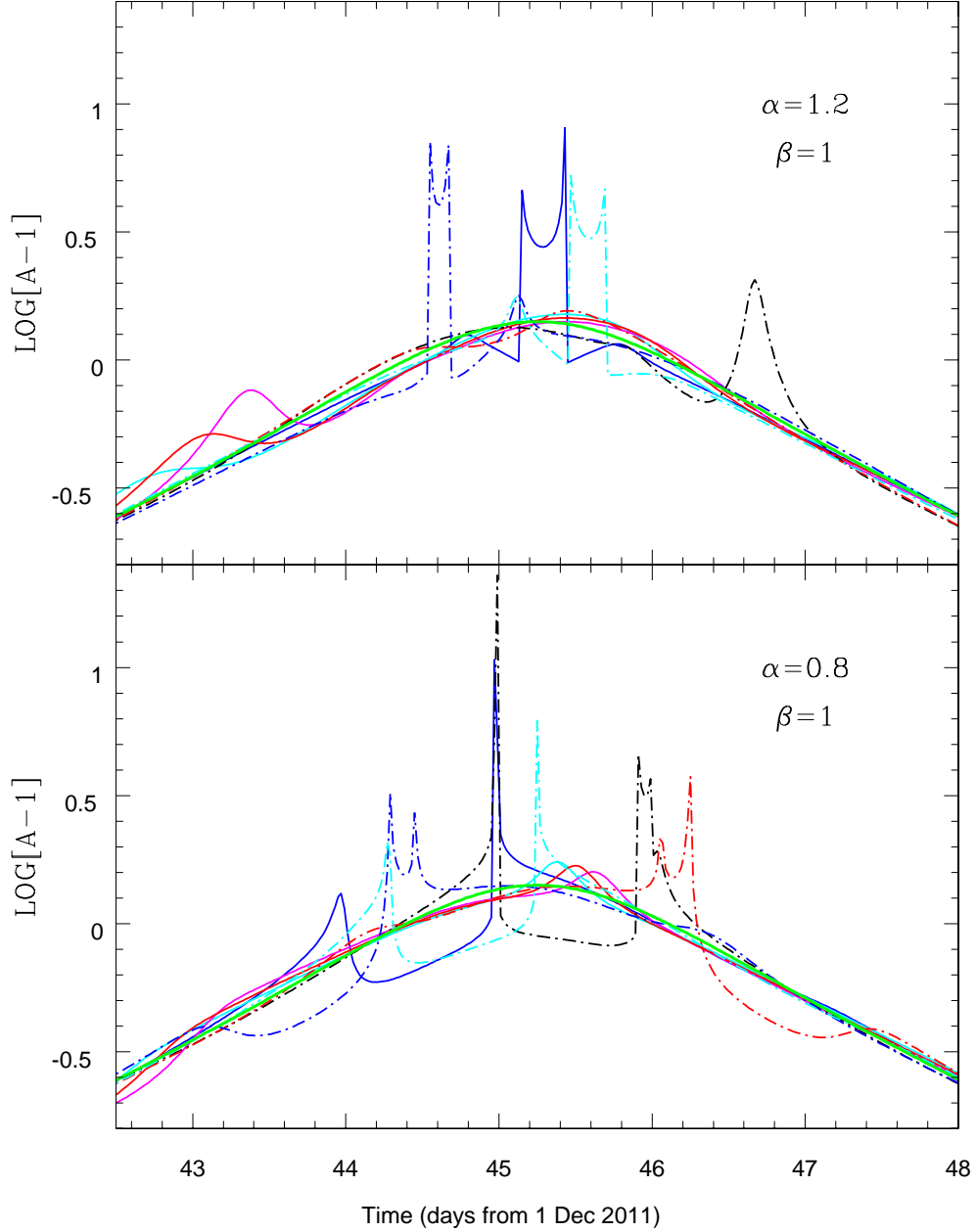


Fig. 3.— Simultaneously plotted light curves for a range of randomly sampled initial phases (in different colours),  $\phi_0$ , for two different values of  $\alpha$  on the 10 mas path. These light curves illustrate the types of features associated with lensing in the resonant zone. Caustic crossings can cause very sharp increases in magnification that are easily detectable, but the smoother curves demonstrate that significant deviations can occur even when caustics are not crossed. Ten separate light curves are plotted in each panel. The fact that a large fraction of them exhibit high magnifications and/or significant deviations from the point-lens form shows that the probability of detectable planet-lens distortions is large.

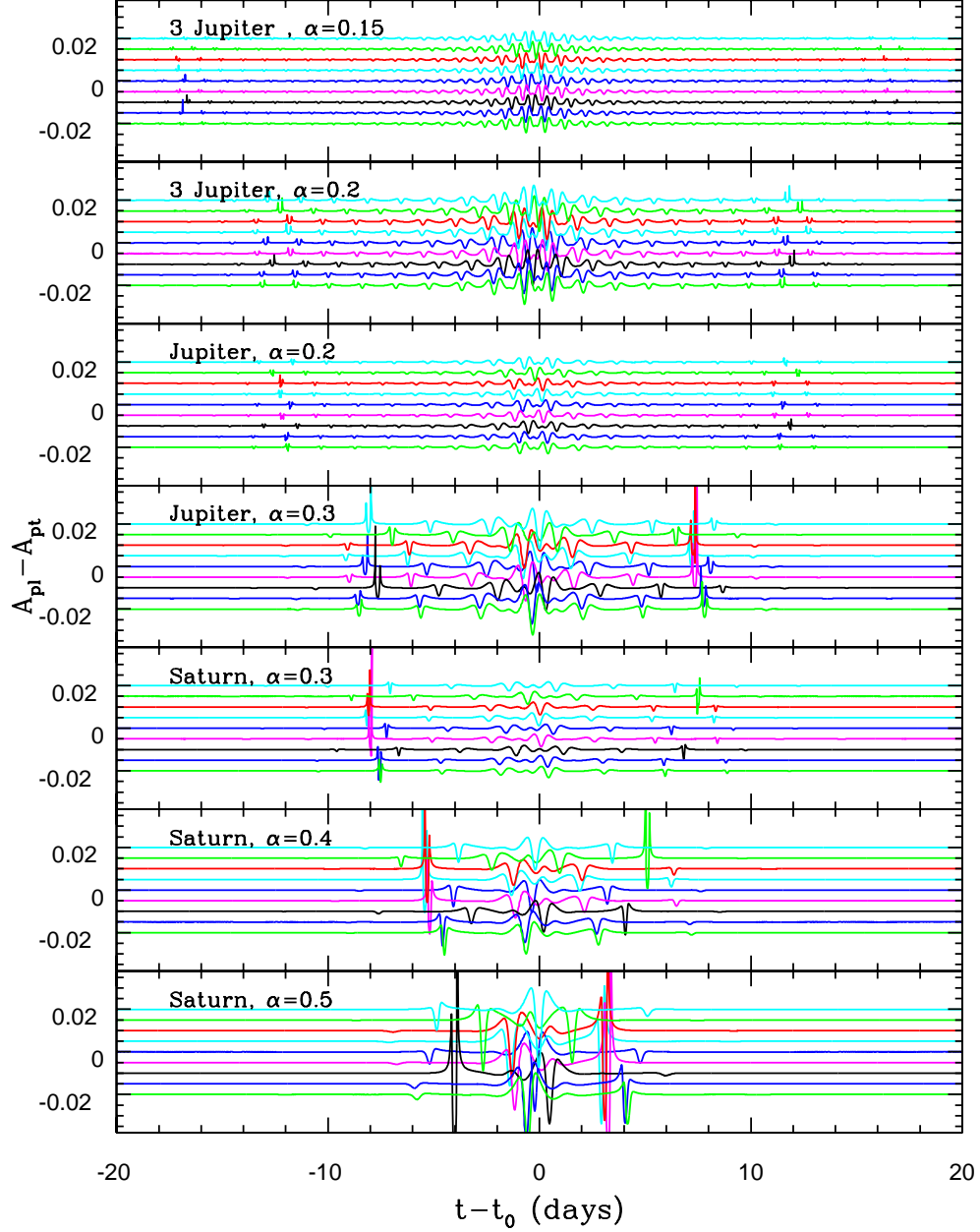


Fig. 4.— The difference between planet-lens ( $A_{pl}$ ) and point-lens ( $A_{pt}$ ) behavior as a function of  $t - t_0$  for close-orbit planets. This illustrates planet effects for a range of orbital separations ( $\alpha$ ) and masses on the 5 mas approach ( $\beta = 0.5$ ). Light curves from different initial orbital phases are shown with vertical offsets for clarity. Small, quasiperiodic deviations from single lens behaviour are observed, and there is increased activity in the region of  $u \sim 1/\alpha - \alpha$ , near the beginning and end of the variability pattern. The deviations close to  $t_0$  are caused by the effect described in §4.4.

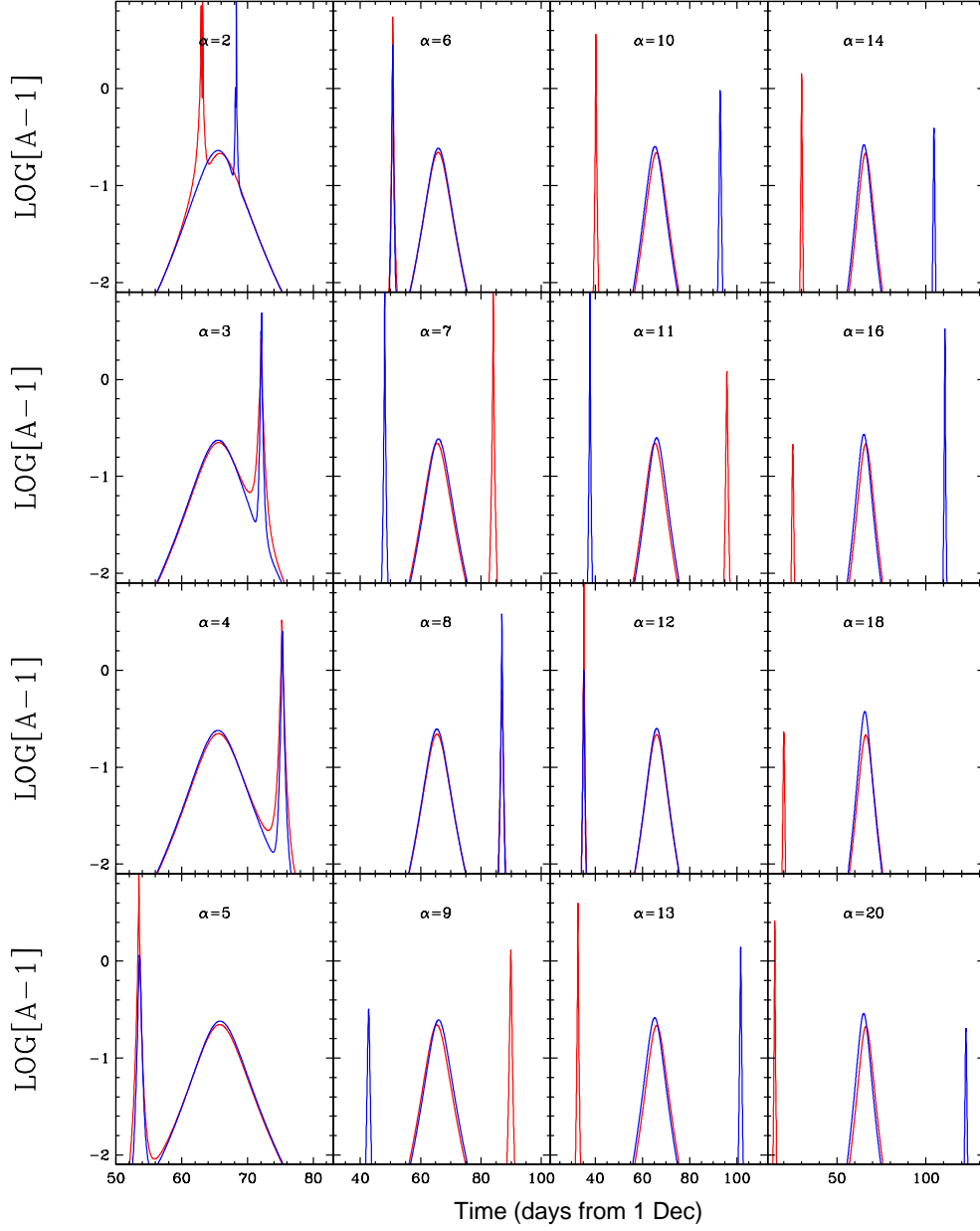


Fig. 5.— Wide orbit planets,  $\beta = 1$ . Simulated light curves for a variety of orbital separations for a Jupiter-mass planet. Red corresponds to clockwise orbits and blue corresponds to counterclockwise. The wider the orbit, the larger the time between the short-duration planet-lens event and the more perturbed the stellar-lens event. This supports the hypothesis that planetary events can be seen over a wide range of dates depending on the orbital separation, up to several months before and after the primary (stellar) event.



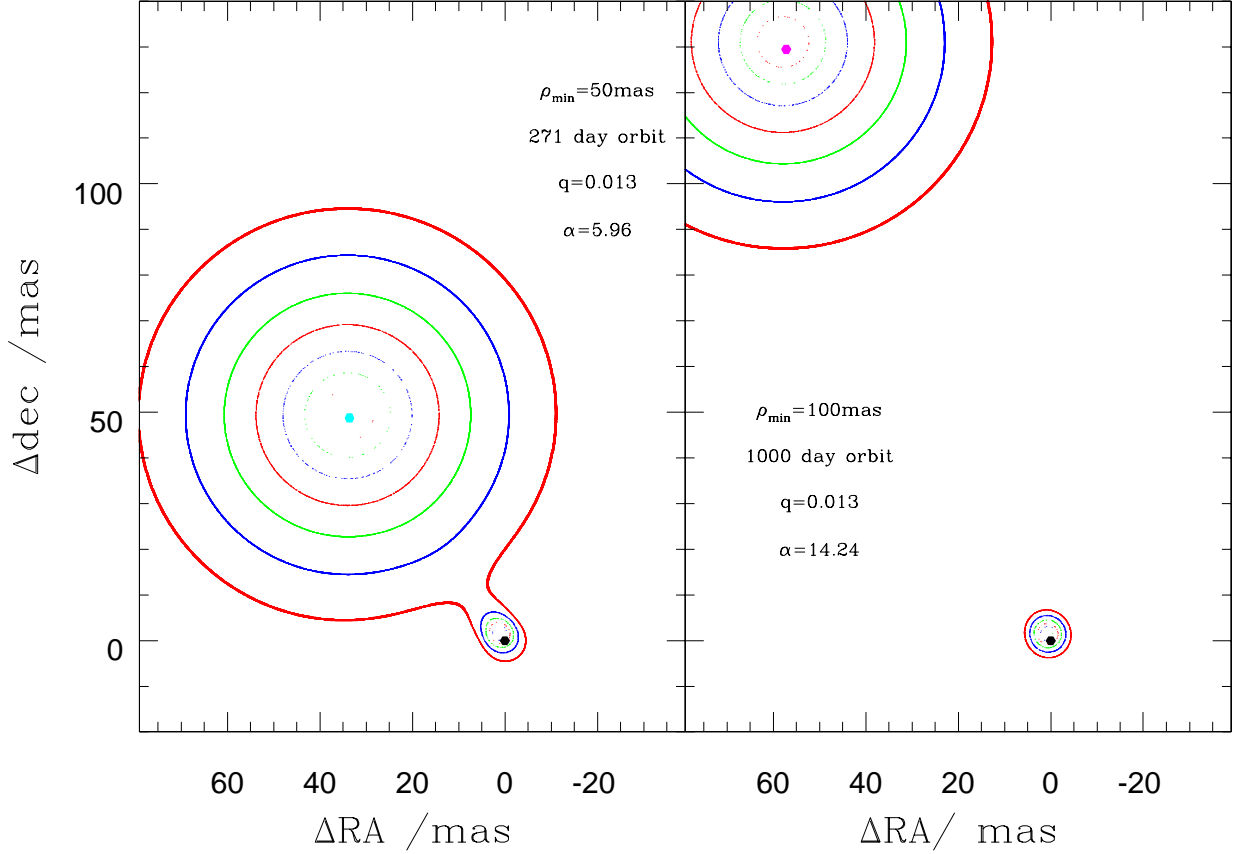


Fig. 6.— Isomagnification contours for two different wide orbits. *Left-hand Panel:*  $\alpha = 5.96$ , corresponding to a 271 day orbit, and *Right-hand Panel:*  $\alpha = 14.2$ , corresponding to a 1000 day orbit. We show each system at a time when the position on the sky of both the planet and the source star is (0,0). The planet produces an independent event by lensing the source star. The isomagnification contours associated with the planet can be clearly identified, and the perturbation in both the position and size of the contours can be seen. The outer red contour corresponds to a magnification  $(A-1) = 0.01$ , and the magnification associated with each contour increases by a magnitude increment (a factor of  $\sim 2.5$ ) as they get closer to the lens. (Note that the isomagnification contours associated with the planet are significantly influenced by VB 10 for  $\alpha = 5.96$ ; for the wider orbit the effect of VB10 on the region around the planet is smaller.

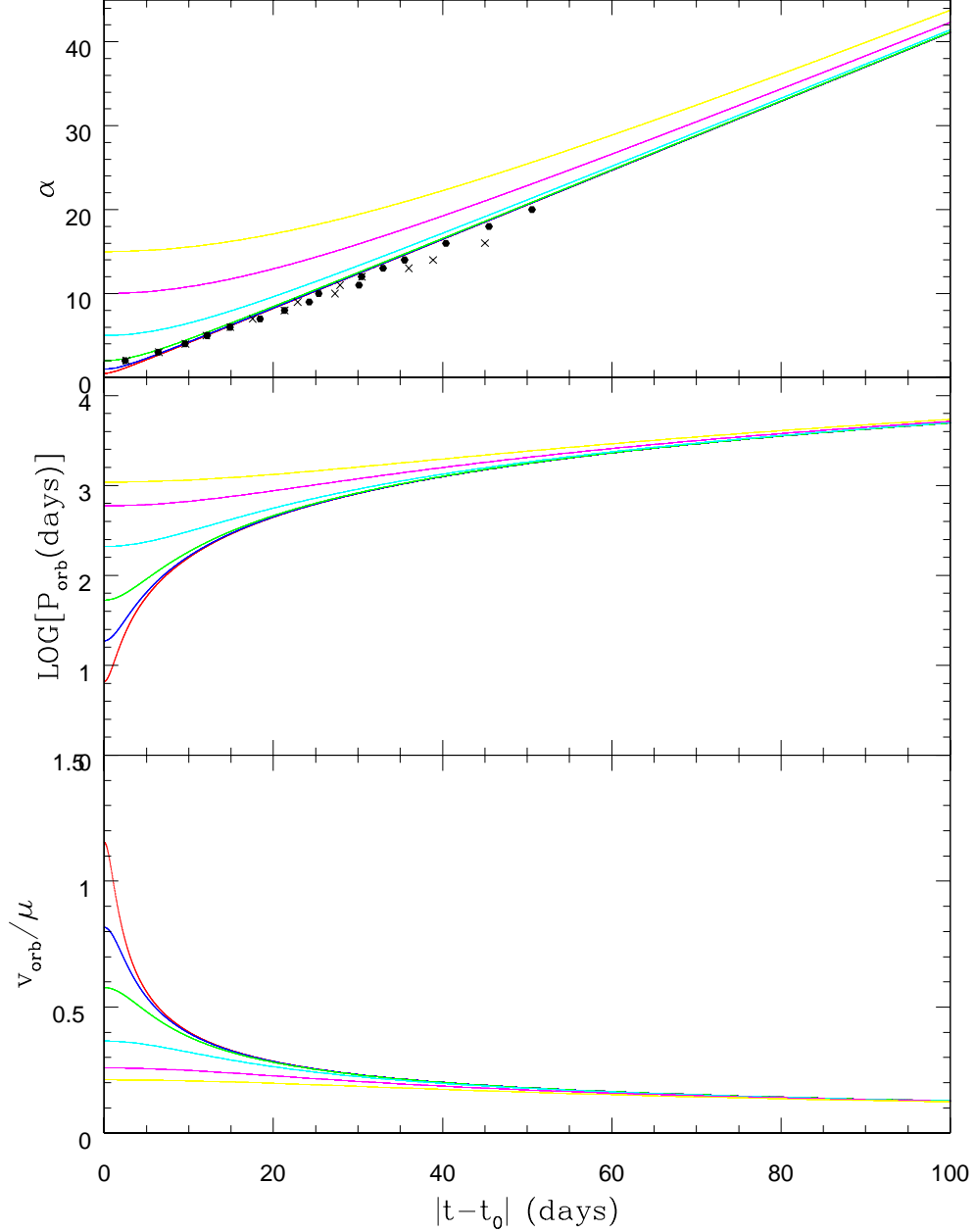


Fig. 7.— The times at which events might occur in the wide regime, plotted with  $\alpha$ ,  $\log(P_{\text{orb}})$  and the ratio between the orbital speed and the proper motion,  $v_{\text{orb}}/\mu$ , respectively. The colors R, B, G, C, M, Y correspond to distances of closest approach of 5, 10, 20, 50, 100 and 150 mas ( $\beta = 0.5, 1, 2, 5, 10, 15$ ) respectively. This uses the approximation of a straight line approach described in Equation 3. The filled hexagons (clockwise) and crosses (counterclockwise) show some actual times of events from simulations, showing the approximation produces reasonable results.

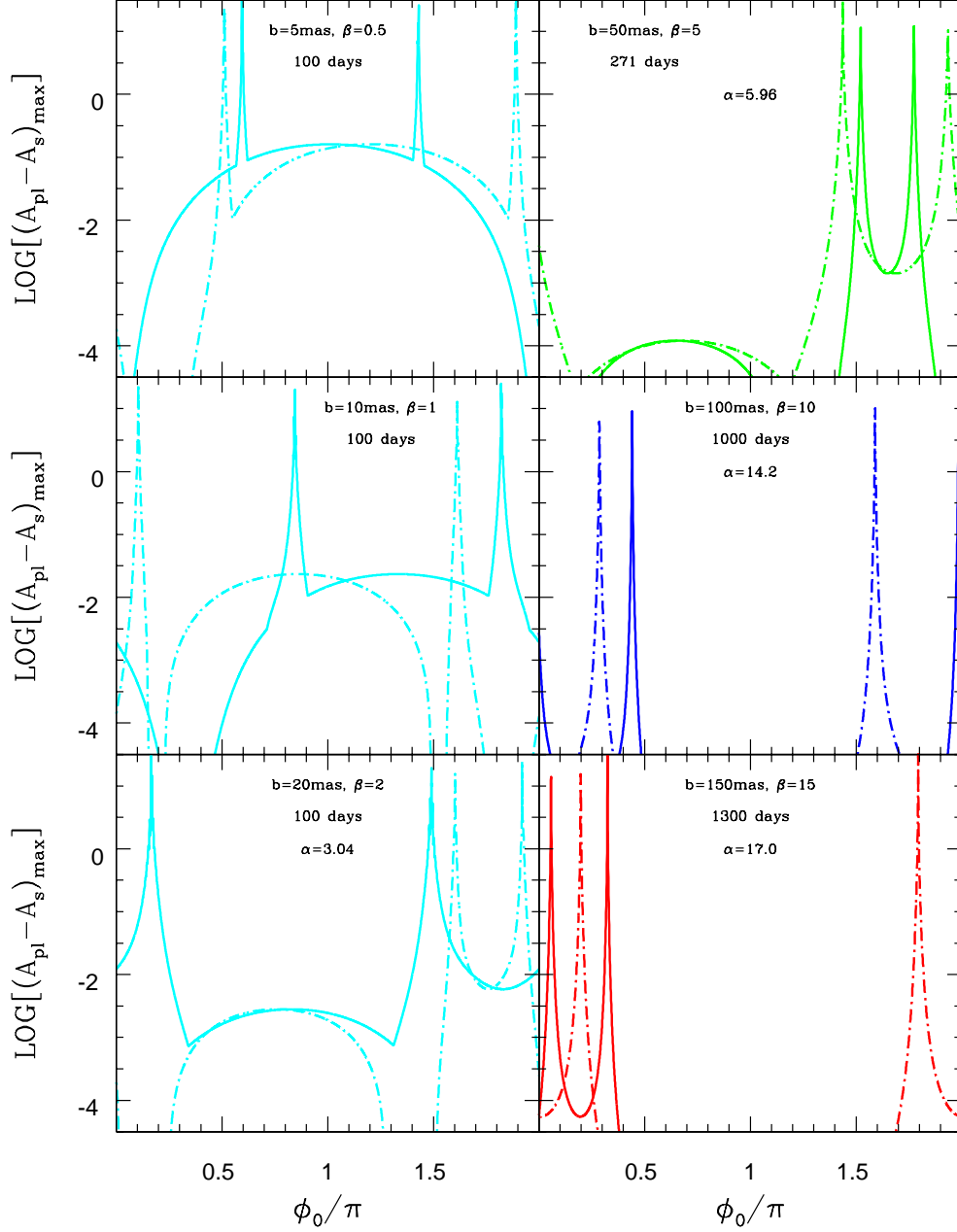


Fig. 8.— Logarithm (base 10) of the maximum difference between the planet-lens and single-lens magnification is plotted as a function of initial orbital phase  $\phi_0$ . This considers a hypothetical case where a Jupiter mass planet orbits VB 10 with periods of 1300 days (red), 1000 days (blue), 271 days (green), and 100 days (cyan). Six different paths are considered, each denoted by their approximate distance of closest approach. Sharp spikes correspond to the planet coming close to the source star. This is for circular, face-on orbits with filled and dashed lines corresponding to clockwise and counterclockwise orbits respectively.

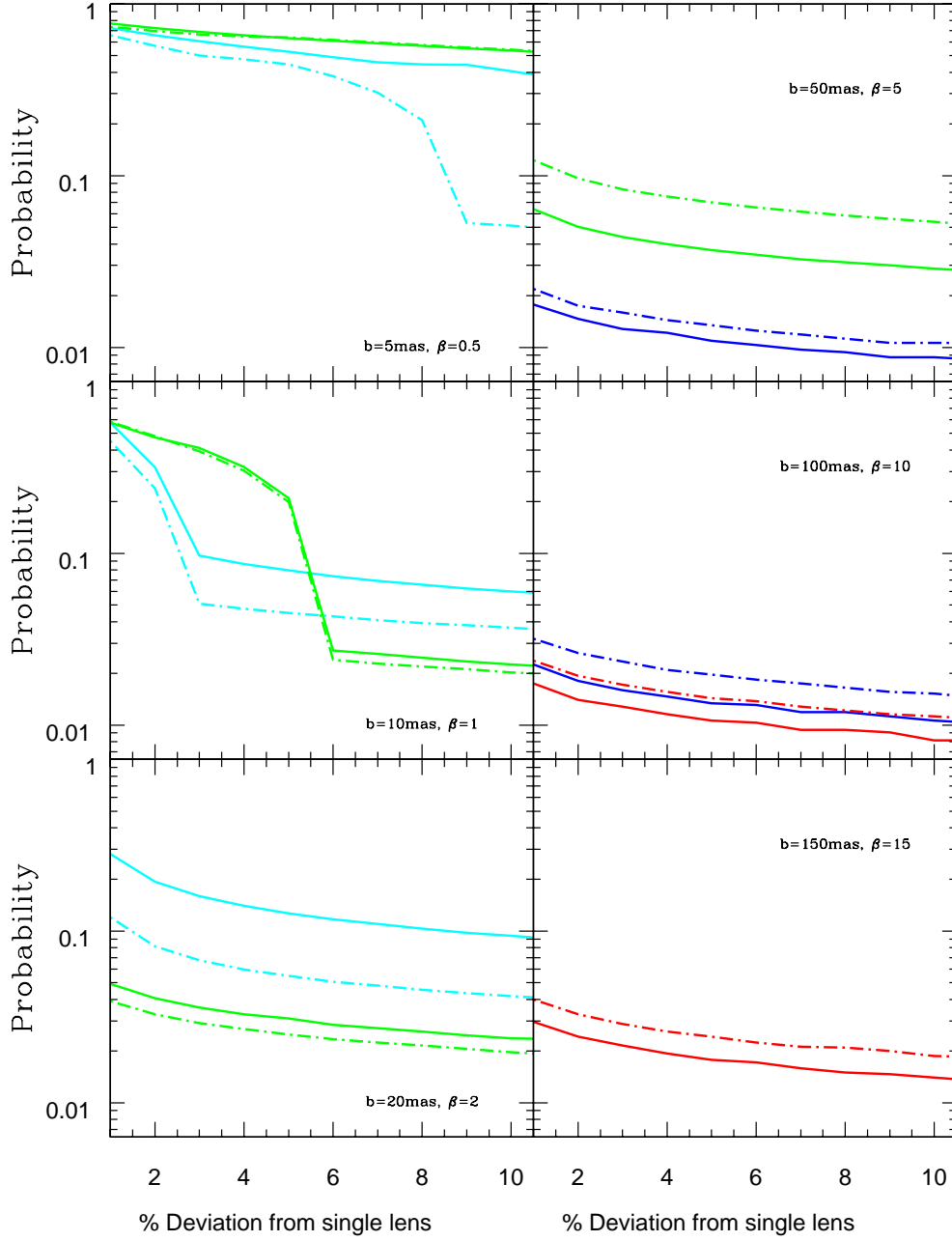


Fig. 9.— Probability that a deviation of a particular size will occur for each of the six paths shown in Figure 1. Probabilities are calculated in the hypothetical cases where a 1 MJ planet is present in orbit around VB 10, on orbital periods of 1300 days (red), 1000 days (blue), 271 days (green), and 100 days (cyan). This is for circular, face on systems with filled and dashed lines corresponding to clockwise and counterclockwise orbits respectively.

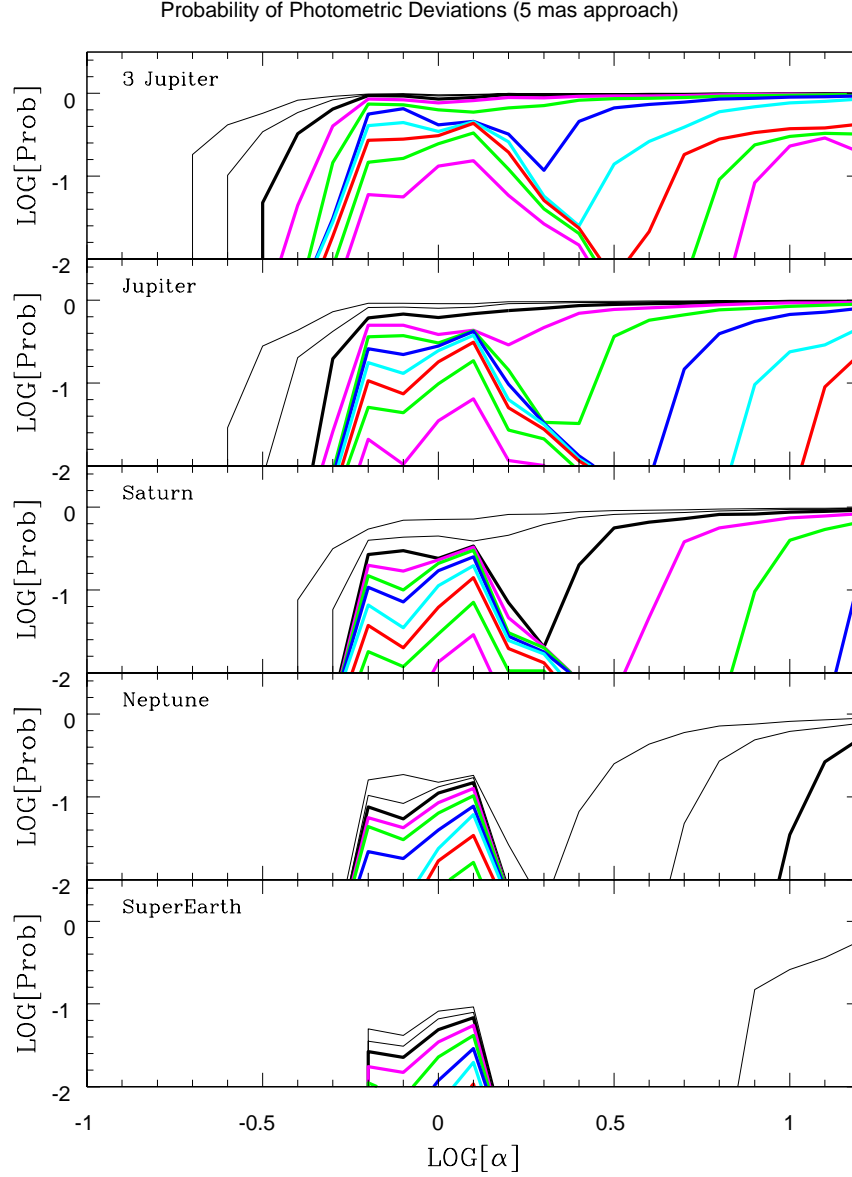


Fig. 10.— Probability of detecting an event exhibiting a photometric deviation of a particular magnitude, versus  $\alpha$ . Each curve corresponds to a specific magnitude of the deviation: 0.01 for the outer thin black line, and increasing by a factor of two for each line below. For this approach ( $b = 5$  mas,  $\beta = 0.5$ ), we see lensing in all three regimes, with particularly high probabilities in the resonant regime. For wide orbits we see a large probability of separate short-duration events for  $\alpha \sim 2$ , especially for more massive planets. This probability falls off simply as  $\alpha$  increases. The increase in probability as  $\alpha$  continues to increase is associated with the wobble of the central star (see §3.4). It is clear that more massive planets are more likely to be detected, as we would expect.

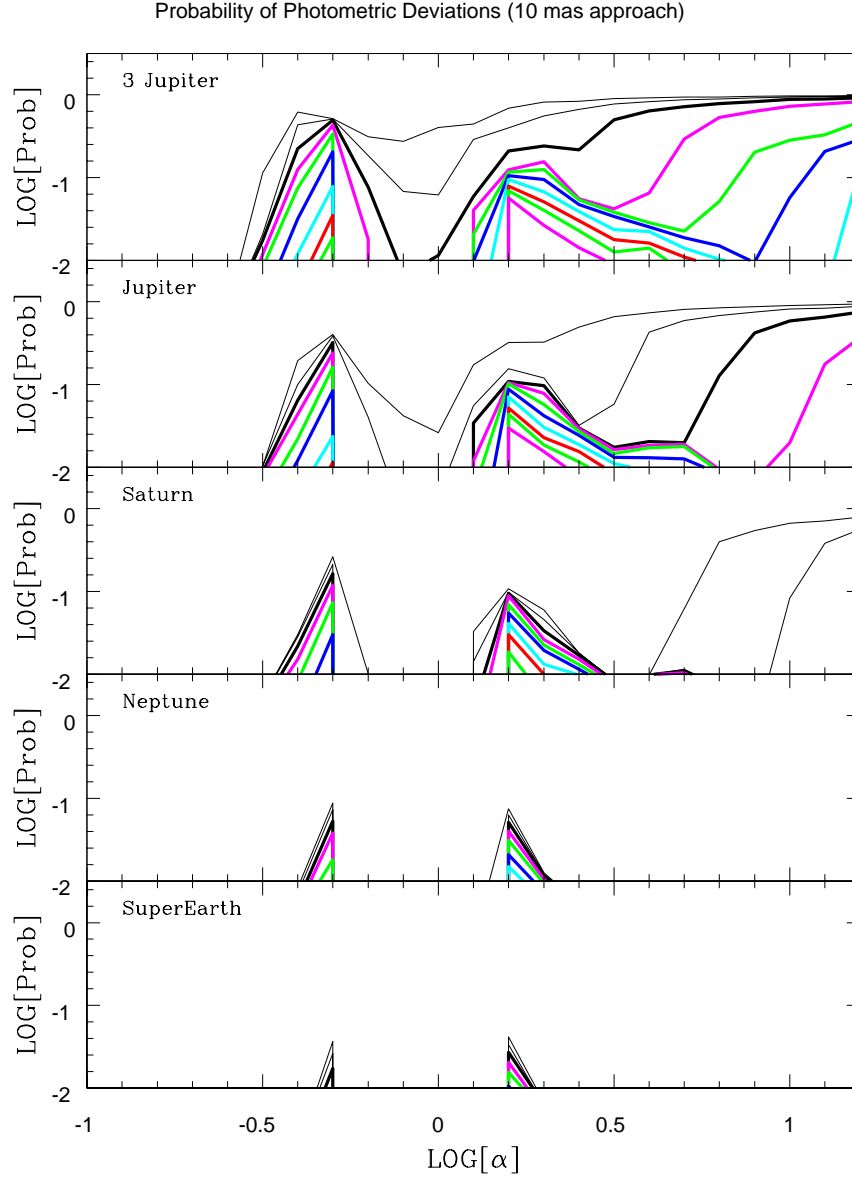


Fig. 11.— The plotted quantities are the same as Figure 13, but for the 10 mas path ( $\beta = 1$ ). Two differences between the  $\beta = 1$  approach of this figure and  $\beta = 0.5$  approach of Figure 13 are noteworthy. First, the amount of activity in the zone for resonant lensing is significantly decreased. Second, there are fewer deviations associated with the wide orbit effects produced by the stellar wobble, since the star produces a smaller magnification in this case.



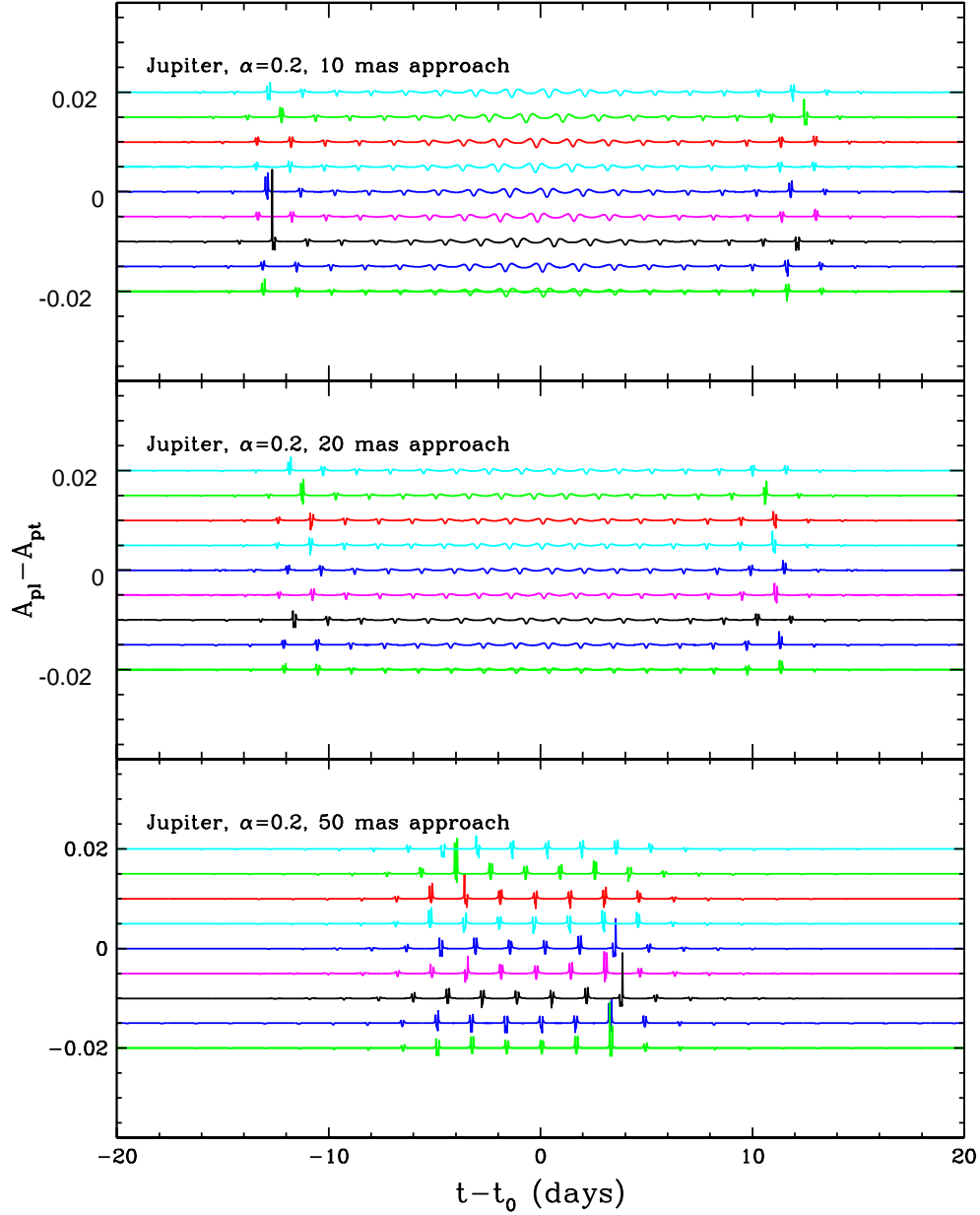


Fig. 12.— The difference between planet-lens ( $A_{pl}$ ) and point-lens ( $A_{pt}$ ) behavior as a function of  $t - t_0$ , analogously to Figure 4.. This illustrates close-orbit planet effects for  $\alpha = 0.2$ , for a Jupiter-mass planet and  $b = 5, 10, 20$  mas ( $\beta = 1, 2, 5$ ). The plots for different phases are separated out in magnification space so the deviations can be seen, so the y axis should be seen as a relative scale only. Small, quasiperiodic deviations from single lens behaviour are produce, and there is increased activity in the region of  $u \sim 1/\alpha - \alpha$ , near the beginning and end of the periodic sequence. The deviations close to  $t_0$  are caused by the effect described in §4.4. The spread in times of events that occurs when the approach is closer can be clearly seen.

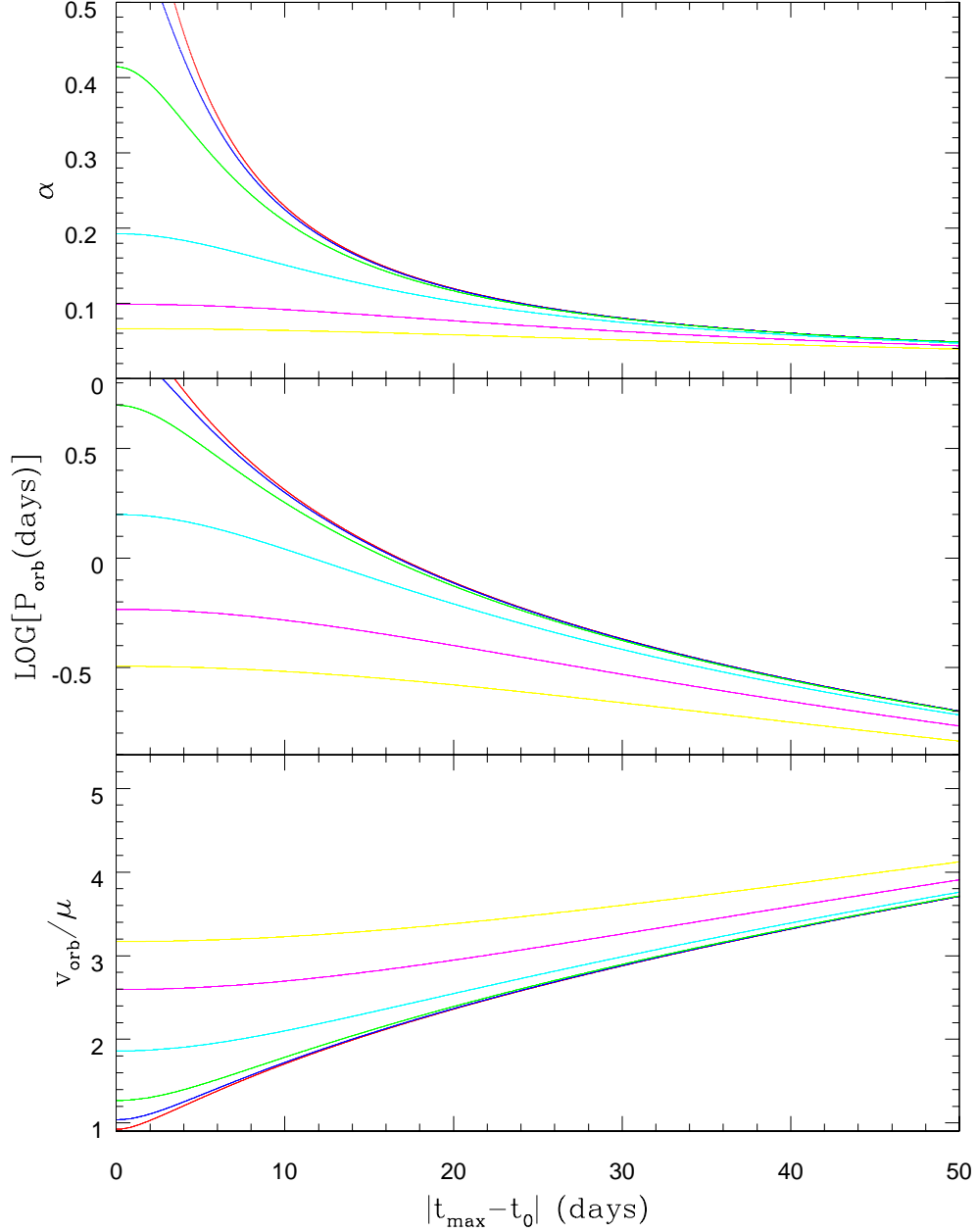


Fig. 13.— The analog to Figure 7 for close orbits. The times at we expect the maximum deviation to occur in the close regime, plotted with  $\alpha$ ,  $\log(P_{\text{orb}})$  and the ratio between the orbital speed and the proper motion,  $v_{\text{orb}}/\mu$ , respectively. The colors R, B, G, C, M, Y correspond to distances of closest approach of 5, 10, 20, 50, 100 and 150 mas ( $\beta = 0.5, 1, 2, 5, 10, 15$ ) respectively. This uses the approximation of a straight line approach described in Equation 6.

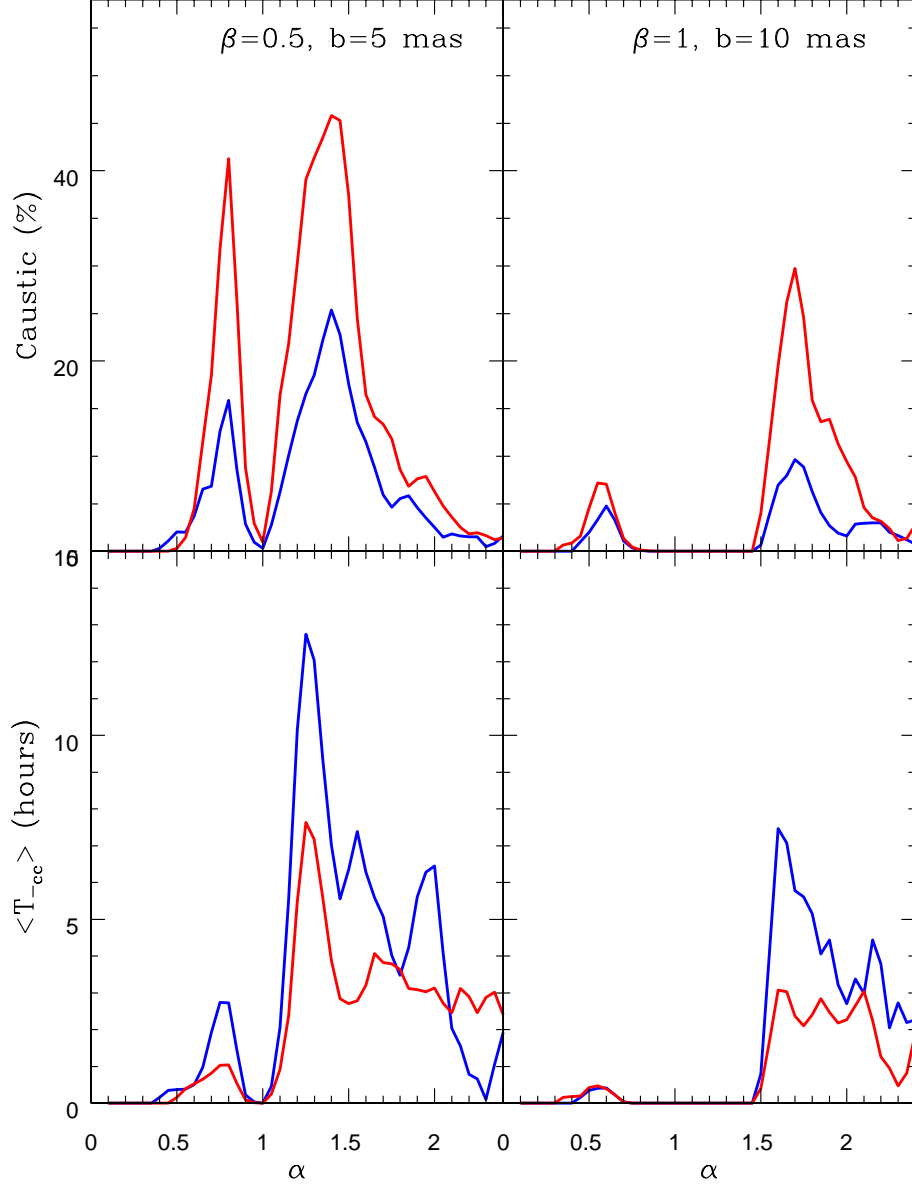


Fig. 14.— Top panels: Percent of all light curves exhibiting caustics, versus  $\alpha$ . Bottom panels: Average time between caustic crossings (while the number of images is 5 and the magnification is larger than 3) versus  $\alpha$ . This graph was produced by a set of simulations generating clockwise (blue curves) and counterclockwise (red curves) orbits for systems in which a  $3 M_J$  planet orbits VB 10. One hundred light curves were generated for each value of  $\alpha$  (starting at 0.05 and increasing in intervals of 0.05) and for each orbital orientation. The results shown were smoothed over three bins in  $\alpha$ . The two panels on the left correspond to  $\beta = 0.5$ , and show that caustics play a more prominent role than for  $\beta = 1$  (right-hand panels).